Electrostatics of the Binding and Bending of Lipid Bilayers: Charge-Correlation Forces and Preferred Curvatures

by

Yang Li

A thesis

presented to the University of Waterloo

in fulfillment of the

thesis requirement for the degree of

Master of Science

in

Physics

Waterloo, Ontario, Canada, 2004

I hereby declare that I am the sole author of this thesis. This is a true copy of the thesis, including any required final revisions, as accepted by my examiners.

I understand that my thesis may be made electronically available to the public.

Abstract

Lipid bilayers are key components of biomembranes; they are self-assembled two-dimensional structures, primarily serving as barriers to the leakage of cell's contents. Lipid bilayers are typically charged in aqueous solution and may electrostatically interact with each other and with their environment. In this work, we investigate electrostatics of charged lipid bilayers with the main focus on the binding and bending of the bilayers.

We first present a theoretical approach to charge-correlation attractions between like-charged lipid bilayers with neutralizing counterions assumed to be localized to the bilayer surface. In particular, we study the effect of nonzero ionic sizes on the attraction by treating the bilayer charges (both backbone charges and localized counterions) as forming a two-dimensional ionic fluid of hard spheres of the same diameter D. Using a two-dimensional Debye-Hückel approach to this system, we examine how ion sizes influence the attraction. We find that the attraction gets stronger as surface charge densities or counterion valency increase, consistent with long-standing observations. Our results also indicate non-trivial dependence of the attraction on separations h: The attraction is enhanced by ion sizes for h ranges of physical interest, while it crosses over to the known D-independent universal behavior as $h \to \infty$; it remains finite as $h \to 0$, as expected for a system of finite-sized ions.

We also study the preferred curvature of an asymmetrically charged bilayer, in which the inner leaflet is negatively charged, while the outer one is neutral. In particular, we calculate the relaxed area difference ΔA_0 and the spontaneous curvature C_0 of the bilayer. We find ΔA_0 and C_0 are determined by the balance of a few distinct contributions: net charge repulsions, charge correlations, and the entropy associated with counterion release from the bilayer. The entropic effect is dominant for weakly charged surfaces in the presence of monovalent counterions only and tends to expand the inner leaflet, leading

to negative ΔA_0 and C_0. In the presence of even a small concentration of divalent counterions, however, charge correlations counterbalance the entropic effect and shrink the inner leaflet, leading to positive ΔA_0 and C_0. We outline biological implications of our results.

Acknowledgments

First of all, I am deeply indebted to my supervisor Prof. Bae-Yeun Ha for his support through detailed and constructive comments throughout my research. I have learned many valuable academic lessons from him, which I am very grateful for. I would also like to thank Prof. Jeff Chen and Prof. Hart Peemoeller who served in my advisory and defense committee, and as well, Prof. Qing-Bin Lu who kindly joined my defense committee. Besides, I am grateful to Sattar Taheri Araghi whose discussion and cooperation benefited me a lot.

I started my master's program at Waterloo two years ago. Canada was the first place I have lived outside of my home country. This was not an easy step for me to take. However, it was the help from the many people I met in Canada that supported me during my study. I would hereby like to thank them for their kindness. These people include my friends from China and my fellow students: Henghua Deng, Weihong Huang, Runqing Jiang, Jianzhen Liang, Yaxi Lin, Dongfeng Liu, Tao Lu, Xiaoming Sun, Zhihui Wang, Guang-an Wei, Li Xiao, Liping Yu, Xiangqun Yuan, Lixin Zhan, Mohammad Ansari, Cedric Beny, Jamal Hassan, Hideo Imamura, Andy Inglot, Hamid Molavianjazi, Sattar Taheri Araghi, Ali Tabei, and Dave Thompson. I would also like to thank Judy McDonnell, the graduate secretary of our department, who has always been glad to help me, and Aaron Levin who helped me edit these acknowledgements.

Finally, I am very grateful to my parents whose patient love has enabled me to complete this work.

Contents

List of Figures

Chapter 1

Introduction

Electrostatic interactions play an important role in many biological processes since biomolecules are typically charged in solution. It was shown that like-charged macromolecules (e.g., DNA and membranes) can attract each other in solutions containing multivalent counterions [1–3]. For example, multivalent polyamines, known to exist in the host bacteria, can facilitate DNA packaging when added to an *in vitro* DNA solution [1, 2]. Adding multivalent counterions, such as Mg^{2+} or Ca^{2+}, can also promote the adhesion of biomembranes [3]. The major components of biomembranes are lipid bilayers, which usually contain a negative net charge, attracting positive ions in solution. It is known that multivalency is required for the attraction [4].

Electrostatic interactions can also be important in membrane bending. One example is the budding of charged vesicles, i.e., closed spherical bilayers. When subject to change in some external conditions, a vesicle buds off from an existing biomembrane, while connected to the biomembrane through a narrow neck [5]. The formation and size of the vesicle is determined by the curvature of the membrane from which it buds. It is known that membrane curvature can be induced by asymmetrical surface charges [6]. Thus the

study of the underlying electrostatic mechanism of bilayer bending is crucial to better understanding of the budding transition.

Another example that involves electrostatics induced bending is the diversity of red blood cell (RBC) shapes. It has been known for many years [7] that the shape of RBC can be transformed into various other shapes depending upon solution conditions such as salt concentration, pH, and the presence of cholesterol [8, 9, 11]. The various RBC shapes can be related to electrostatic interactions, since the charge asymmetry of RBC membranes induces curvature: The inner leaflets of RBC membranes are rich in anionic lipids while the outer ones are neutral. Such charge asymmetry can induce membrane bending in a solvent-dependent way, resulting in shape changes.

1.1 Structure of a biomembrane

Amphiphilic molecules such as phospholipids can self-assemble into a variety of structures in aqueous solutions. A typical lipid comprises a polar head group and a nonpolar tail of hydrocarbon chains. At a water-oil interface, lipid molecules tend to form a monolayer with the hydrophilic head group immersed in water and the hydrophobic tail in oil. In a single solvent (e.g., water), these molecules can form a (closed) bilayer consisting of two opposing monolayers. Note not all kinds of lipids tend to form bilayers. Lipids with double chains are more likely to do so. The hydrophobic chains tend to stay inside the bilayer to avoid contact with water, leaving head groups exposed to water.

A key component of a biomembrane is a lipid bilayer. Most lipids found in biomembranes are phospholipids, including phosphatidylserine (PS), phosphatidylglycerol(PG), phosphatidylcholine (PC) and phosphatidylethanolamine (PE), characterized by their chains and head groups. Some of them are charged (PS) at neutral pH, while others are electrically neutral (PC). Biomembranes are usually immersed in salty solution containing

mobile counterions (i.e., ions carrying opposite charges to the biomembranes), ions from dissolved salts and other chemical components. The biomembrane and its environment are electrically overall neutral.

In addition to phospholipids, a biomembrane also contains glycolipids, cholesterols, embedded proteins, and glycocalyx, a sugary coat attached to glycolipids and proteins. Due to the complexity of biomembranes, both experiments and theories find it useful to consider pure lipid bilayers. Theoretically, such pure lipid bilayers are further simplified: the molecular details of lipid head groups are ignored; the layer of head groups is considered as forming a two-dimensional surface. This surface has a planar charge density if the bilayer contains charged lipids. The thickness of the bilayer is determined by the hydrocarbon chain length (about 2 nm). Crude as it is, this simplification can be used to study important features of electrostatics of the system, as will be seen in the remainder of the thesis.

1.2 Distribution of counterions between two like-charged plates

Two like-charged plates usually repel each other electrostatically in solution. However, they can attract each other under special conditions [2]. In this case, counterions are expected to play a key role. For negatively charged plates, they are cations such as $[Na^+]$ and $[Ca^{2+}]$. Being mobile, counterions may stay close to the bilayer at low temperatures, or move away from it at high temperatures. To get some hint about the nature of such attraction, we find it useful to study the spatial distribution of counterions between two charged plates in solution.

The fundamental equation used to calculate the distribution of counterions is the Poisson-Boltzmann equation. The Poisson equation relates charge density to the electrical

potential:

$$\nabla^2\psi(\mathbf{r}) = -\frac{4\pi Ze}{\epsilon}\rho(\mathbf{r}), \tag{1.1}$$

where Z is the counterion valency, e is the elementary unit of charge, ϵ is the dielectric constant of water, and $\psi(\mathbf{r})$ and $\rho(\mathbf{r})$ are the electrical potential and the number density of counterions at position $\mathbf{r}$, respectively. The chemical potential of counterions can be written as

$$\mu(\mathbf{r}) = Ze\psi(\mathbf{r}) + k_BT\ln\rho(\mathbf{r}), \tag{1.2}$$

where k_B is the Boltzmann constant and T is the temperature. In equilibrium, the chemical potential is uniform everywhere. If we choose $\psi(\mathbf{r_0}) = 0$ and $\rho(\mathbf{r_0}) = \rho_0$, the number density of counterions follows the Boltzmann distribution:

$$\rho(\mathbf{r}) = \rho_0 \mathrm{e}^{-\frac{Ze\psi(\mathbf{r})}{k_BT}}, \tag{1.3}$$

This, when combined with Eq. 1.1, becomes the Poisson-Boltzmann equation,

$$\nabla^2\psi(\mathbf{r}) = -\frac{4\pi Ze}{\epsilon}\rho_0 \mathrm{e}^{-\frac{Ze\psi(\mathbf{r})}{k_BT}}. \tag{1.4}$$

We now consider two parallel plates perpendicular to z-axis, separated by a distance h, immersed in solution where only counterions are present. Each plate is negatively charged with surface charge density $\sigma = -e\sigma_0$. If we choose $z = 0$ in the middle of the two plate, and $\rho(0) = \rho_0$, the Poisson-Boltzmann equation can be solved and $\rho(z)$ is given by [10]

$$\rho(z) = \frac{\rho_0}{\cos^2(Kz)}, \tag{1.5}$$

where

$$K^2 = \frac{(Ze)^2\rho_0\ell_B}{2}, \tag{1.6}$$

where $\ell_B = e^2/\epsilon k_BT$ is the Bjerrum length, a length scale at which the electrostatic energy and the thermal energy become comparable, and ρ_0 is given by the boundary

condition

$$\left.\frac{d\psi(z)}{dz}\right|_{z=h/2} = \frac{\sigma}{\epsilon}. \tag{1.7}$$

The distribution reflects the competition between entropy and energy. Entropy favors a uniform distribution, while energy drives counterions to the plates. When the two plates are brought together, the counterions tend to be pulled back to the plates, in effect against entropy. Thus entropy results in repulsion between two plates. To understand how the two plates attract each other, we need to consider two processes: counterion condensation and charge correlation.

1.3 Counterion condensation and charge correlation

For a highly charged plate, electrostatic energy will dominate entropy so that a majority of counterions are located within a thin layer near the plates. The thickness of this layer is typically on the order of the Gouy-Chapman length $\lambda = (2\pi\ell_B\sigma_0)^{-1}$, the length scale beyond which most of surface charges are neutralized. In the limit of high charge densities, λ is much smaller than h, the separation of the two plates. Thus this layer can be considered essentially two-dimensional and counterions are localized to the plates. This is referred to as counterion condensation [12].

Condensed counterions not only neutralize surface charges but also make charge distributions heterogeneous, which become correlated from one plate to the other. On each of the two plates, a positive charge tends to be surrounded by a negative ionic cloud, while a negative charge prefers to be surrounded by a positive ionic cloud. When the two plates get close, a positive rich part on one plate attracts a negative rich part on the other plate, leading to attraction.

1.4 Bending of a bilayer membrane

Lipid bilayers are self-assembled structures. They are soft and flexible, thus exhibiting a rich set of conformational behavior (shapes, undulation, budding). The driving forces for lipid aggregation are weak van der Waals, hydrophobic and screened electrostatic interactions, i.e., non-covalent bonds. Change in solution conditions such as ion concentration or valency will not only influence interactions between bilayers but also affect forces between lipids and thus modify the area and shape of the bilayer. Therefore, we shall study these weak interactions in order to understand the conformational properties of bilayers. In particular, we focus on the effect of electrostatic interactions on bilayer bending. To this end, we treat a bilayer as a fluid-like structure, composed of two monolayers. Subject to forces, it can undergo two types of deformations: in-plane deformation, such as compression or stretching, and out-of-plane deformation, i.e., bending. Normally, the two types of deformation are coupled to each other due to the finite thickness of the bilayer: bending makes one leaflet compressed and the other stretched out.

Bending of a bilayer is described by its preferred curvature, which has two different physical origins: first, the intrinsic spontaneous curvatures of two monolayers determine the spontaneous curvature of the bilayer; second, the relaxed area difference between the inner and the outer monolayers give rise to a unique contribution to the preferred curvature. These two effects combine into an effective curvature (preferred curvature) [13]. This quantity can be measured experimentally [14, 15].

1.5 About this thesis

In Chapter 2, we will present a theoretical approach to attractions between like-charged bilayers with neutralizing counterions. Counterions are assumed to be localized to the

bilayer surfaces. The attractions arise from charge correlations between surface charge and counterions. In particular, we study the effect of nonzero ionic sizes on the attraction.

The relaxed area difference between two leaflets of an asymmetrically charged bilayer is calculated in Chapter 3. The relaxed area difference is determined by interactions on the lipid-water interface and can be modified by electrostatic forces between surface charges and counterions.

Based on a microscopic model that describes the spontaneous curvature of a monolayer, we develop in Chapter 4 a formalism to calculate the spontaneous curvature of an asymmetrically charged bilayer. In particular, we focus on the interplay between charge asymmetry and counterion valency. We briefly discuss biological implications of our result.

Chapter 2

Nonzero ionic size and charge-correlation forces between bilayers

2.1 Introduction

Counterion-induced attractions between like charges are ubiquitous in biology, as a large class of biological processes rely on these attractions [1, 2, 16–18]. Some viruses use multivalent counterions in their host cells to package their DNA, which carries a negative charge in aqueous solution [1, 2]. These attractions are also responsible for the formation of bundles of other kinds of stiff polyelectrolytes such as microtubules and actin filaments [16], which are crucial to the mechanical properties of living cells. Membrane adhesion can also be promoted by multivalent counterions such as Mg^{2+} and Ca^{2+} [3].

Since the mean field approach of Poisson-Boltzmann theory always predicts repulsion between like charges, the electrostatic mechanism behind these observations has

been a subject of intensive research in the past few decades, producing a number of seemingly-distinct theoretical approaches [12, 19–30]. In all these approaches, the attraction arises from correlations between counterions, especially those in the close proximity of their co-ions. The major difference between them lies in the way they capture ion correlations. For example, an integral-equation method has been used to account for counterion-density correlations [19, 20]. This approach relies on an approximation scheme, namely a closure for pair correlation functions, and often requires heavy numerical analysis. In more analytical treatment [23,28], charge fluctuations are captured at the Gaussian level. For unscreened planar cases (e.g., charged bilayers in a low-salt limit), the electrostatic pressure shows universal power-law behavior at large separations [20,21,23]: $\Pi(h/\lambda \to \infty) \equiv \Pi_\infty \sim -k_B T/h^3$, where λ is the Gouy-Chapmann length, a length scale within which most counterions are localized (see the more precise definition of λ below Eq. 2.5). This result is independent of surface charge densities and counterion valency. In a low-temperature picture [27], the attraction is reminiscent of a strong charge correlation that drives the system into an ionic crystal at zero temperature and decays exponentially with h. There are some variations of this approach [29, 30], but they do not deviate in spirit significantly from it. More recently, it's been shown that a more complete theory should incorporate both kinds of behavior [31,32]: the power-law pressure and the exponential pressure. Depending on surface charge densities or temperature, the short-ranged, exponentially-decaying pressure can be dominant at short separations, but it should cross over to the power-law pressure as h increases. Finally, strong-coupling (SC) theory has been proposed that becomes asymptotically exact in the strong coupling limit (i.e., low temperatures, high surface charge densities, and large counterion valency) [33,34]. While the SC approach is supported by simulations in the SC limit [33,34], the relation between the low temperature picture and the SC approach has yet to be explored.

Despite all this effort, the problem of counterion-induced attraction still remains chal-

lenging. Many existing (analytically tractable) theoretical approaches [12, 17, 20, 22–30] rely on a common approximation for charges: point charges. While some aspects of nonzero ionic sizes were discussed in a more numerical treatment in the literature (see, for example, Ref. [20]), a more comprehensive picture is highly desirable. In this chapter, we develop a more analytical approach that will provide a more direct picture of how finite ionic sizes influence the electrostatic attraction. We discuss the effects of ionic sizes on the electrostatic attraction between like-charged surfaces. We will use two-dimensional Debye-Hückel (DH) theory (i.e., linearized Poisson-Boltzmann theory) for highly charged surfaces with neutralizing counterions assumed to be localized to the surface—delocalized counterions will not be taken into account. Here, both backbone charges and counterions are modeled by hard spheres of the same diameter D as in the restrict primitive model [38]. The main advantage of our approach lies in that it provides a simple physical picture for the attraction without being complicated by other competing effects. We find that the effect of finite D is dramatic: In contrast to Π_∞, which is independent of σ (planar charge densities) or Z (counterion valency), the DH pressure for $D > 0$ can be sensitive to σ and gets stronger as σ or Z increases in magnitude (unless h is too small). This is intriguing as it indicates that ionic sizes influence σ (or Z)-dependence of the pressure. Our results are consistent with long-standing observations of stronger attractions for higher σ_0 or larger Z [20, 27, 35, 36]. Our results also indicate non-trivial dependence of the attraction on h. While the attraction reduces to the limiting pressure Π_∞ in the limit $h \to \infty$, it shows D dependence for h ranges of physical interest. The attraction is enhanced by ionic sizes for moderately large h ($h \gtrsim 5$Å), but it approaches a finite value as $h \to 0$. The ionic size enhances a charge polarity, leading to a stronger attraction unless h is too small. On the other hand, the free energy (per area) for $D > 0$ is finite, leading to a finite attraction (per area) as $h \to 0$. However, our approach may leave out strong coupling between ions that becomes important at low temperatures and

can be considered as complimentary to SC theory [33, 34].

2.2 Model and interaction free energy

We consider two parallel surfaces perpendicular to z-axis, a distance h apart. Each surface is assumed to be negatively charged with the same backbone charge density $\sigma \equiv -e\sigma_0$. For sufficiently large σ_0 (> 0), the Gouy-Chapman length λ, a length scale beyond which each surface is neutralized, is smaller than typical ion sizes. In this case, it is useful to classify counterions into two subclasses [12,17]: "condensed" and "free". In this simplified picture, both backbone charges and condensed counterions are approximated to lie in the same plane of the surface—they give rise to in-plane charge fluctuations that become correlated from one surface to the other, leading to an attraction. For simplicity, we will not include free (delocalized) counterions. As a result, we limit ourselves to unscreened cases only, i.e., $\kappa \to 0$, where κ^{-1} is the Debye screening length. Here, we adopt the so called restricted primitive model [37, 38] of ions and treat both backbone charges and condensed counterions as hard spheres of the same diameter D, carrying charge at the center. As a result, the interaction between two charges q and q' separated by a distance r assumes the following form [38]:

$$U(r) = \begin{cases} \infty, & r < D \\ \frac{qq'}{\epsilon r} & r > D \end{cases} . \tag{2.1}$$

Here the dielectric constant ϵ is assumed to be constant throughout the system (thus suppressing dielectric discontinuity) and will be taken to be that of water. Furthermore, we assume that condensed counterions have the same valency Z. This is reasonable, since multivalent counterions are preferentially adsorbed onto a highly charged surface [10].

In order to treat condensed counterions and backbone charges on equal footing, we use $Z_\alpha e$ to denote the charge on the two different kinds of ions: $Z_\alpha = Z$ for counterions and

$Z_\alpha = -1$ for backbone charges. The overall electric neutrality then requires $\sum_\alpha Z_\alpha \sigma_\alpha = 0$ [39] (Note $Z_\alpha e \sigma_\alpha$ is the surface charge density of the αth kind of ions). Most of crucial properties of the resulting system can be studied by holding an ion on one of the surfaces and examining how other ions respond to it [37, 38]. To this end we put an ion of charge Z_α at the origin on surface 1, and calculate the electric potential created by this ion and the surrounding ionic cloud of opposite charge, denoted by $\Psi_j(\mathbf{r})$, where $j(= 1, 2)$ runs over surfaces at $z = 0$ and h, respectively. The electrostatic potential at position $\mathbf{r}$ is then described by the Poisson-Boltzmann equation:

$$\nabla^2 \Psi(\mathbf{r}) = -\frac{4\pi}{\epsilon} \rho(\mathbf{r}), \tag{2.2}$$

and

$$\rho(\mathbf{r}) = \begin{cases} Z_\alpha e \delta(\mathbf{r}) & r < D \\ e\left[\delta(z) + \delta(z-h)\right] \sum_\alpha \sigma_\alpha Z_\alpha \mathrm{e}^{-\beta Z_\alpha e \Psi(\mathbf{r})} & r > D \end{cases}, \tag{2.3}$$

where $\beta = 1/k_B T$ and $\delta(z)$ is the Dirac δ function, which arises as counterions are localized to the surfaces.

In Debye-Hückel theory, the above equation at $r > D$ is linearized [38] as follows:

$$\mathrm{e}^{-\beta Z_\alpha e \Psi(\mathbf{r})} \simeq 1 - \beta Z_\alpha e \Psi(\mathbf{r}), \tag{2.4}$$

such that

$$\begin{aligned} \rho(\mathbf{r}) &= e\left[\delta(z) + \delta(z-h)\right] \left[\sum_\alpha \sigma_\alpha Z_\alpha - \beta e \Psi(\mathbf{r}) \sum_\alpha \sigma_\alpha Z_\alpha^2 \right] \\ &= -\frac{\epsilon}{2\pi\lambda} \Psi(\mathbf{r}) \left[\delta(z) + \delta(z-h)\right]. \end{aligned} \tag{2.5}$$

where $\lambda^{-1} = 2\pi \ell_B \sum_\alpha Z_\alpha^2 \sigma_\alpha$ and $\ell_B = e^2/\epsilon k_B T$. Note we have used the condition $\sum_\alpha Z_\alpha \sigma_\alpha = 0$. The validity of this approach can be checked *a posteriori*–see the relevant discussion below Fig. 2.4. The overall neutrality requires $\lambda^{-1} = 2\pi \ell_B (Z+1) \sigma_0$. The electrostatic potential is then given by the following differential equation:

$$\nabla^2 \Psi(\mathbf{r}) = \begin{cases} -\frac{4\pi}{\epsilon} Z_\alpha e \delta(\mathbf{r}) & r < D \\ \frac{2}{\lambda} \Psi(\mathbf{r}) \left[\delta(z) + \delta(z-h)\right] & r > D \end{cases}, \tag{2.6}$$

Here we are particularly interested in the electric potential in the plane of the surface: $\psi_1(\mathbf{r}_\perp) \equiv \Psi(\mathbf{r}_\perp, z = 0)$ and $\psi_2(\mathbf{r}_\perp) = \Psi(\mathbf{r}_\perp, z = h)$, where $\mathbf{r}_\perp = (x, y)$. By solving Eq. 2.6, we find, for $r > D$,

$$\begin{aligned}
\psi_1(\mathbf{r}_\perp) &= Av_{11} - \frac{\lambda^{-1}}{2\pi}\int d\mathbf{r}'_\perp \sum_{j=1}^{2} \psi_j(\mathbf{r}'_\perp) v_{1j}(\mathbf{r}'_\perp - \mathbf{r}_\perp) \\
\psi_2(\mathbf{r}_\perp) &= Av_{12} - \frac{\lambda^{-1}}{2\pi}\int d\mathbf{r}'_\perp \sum_{j=1}^{2} \psi_j(\mathbf{r}'_\perp) v_{2j}(\mathbf{r}'_\perp - \mathbf{r}_\perp),
\end{aligned} \tag{2.7}$$

where $v_{ij} = 1/\sqrt{r_\perp^2 + h_{ij}^2}$ and $h_{ij} = h$ if $i \neq j$ and 0 otherwise. The first term of each equation above, Av_{ij}, is the bare interaction between two ions on surface i and j respectively; the second term is the screened interaction. Note here that the integration constant A is not automatically set in the two-dimensional case, in contrast to the corresponding three dimensional case where it is fixed by Gauss' law [37]. If we apply Fourier transform to Eq. 2.7, we can calculate $\psi_1(\mathbf{r}_\perp)$ and $\psi_2(\mathbf{r}_\perp)$. It proves useful to introduce a matrix M defined by matrix elements:

$$M_{ij}(\mathbf{k}_\perp) = \delta_{ij} + \frac{\mathrm{e}^{-h_{ij}k_\perp}}{\lambda k_\perp}. \tag{2.8}$$

Note $\mathrm{e}^{-h_{ij}k_\perp}/k_\perp$ is the Fourier transform of v_{ij}. In terms of this, $\psi_1(\mathbf{r}_\perp)$ and $\psi_2(\mathbf{r}_\perp)$ are given as follows

$$\begin{aligned}
\psi_1(\mathbf{r}_\perp) &= A\lambda \int \frac{d\mathbf{k}_\perp}{(2\pi)^2} \frac{M_{11}(\mathbf{k}_\perp)\left[M_{11}(\mathbf{k}_\perp) - 1\right] - M_{12}^2(\mathbf{k}_\perp)}{\det\left[M(\mathbf{k}_\perp)\right]} \mathrm{e}^{i\mathbf{k}_\perp \cdot \mathbf{r}_\perp}, \\
\psi_2(\mathbf{r}_\perp) &= A\lambda \int \frac{d\mathbf{k}_\perp}{(2\pi)^2} \frac{M_{12}(\mathbf{k}_\perp)}{\det\left[M(\mathbf{k}_\perp)\right]} \mathrm{e}^{i\mathbf{k}_\perp \cdot \mathbf{r}_\perp},
\end{aligned} \tag{2.9}$$

The θ integral in the above equations can be carried out:

$$\frac{1}{2\pi}\int d\theta\, \mathrm{e}^{i\mathbf{k}_\perp \cdot \mathbf{r}_\perp} = J_0(k_\perp r_\perp), \tag{2.10}$$

where $J_0(x)$ is the zeroth-order Bessel function of the first kind. From this we obtain

$$\begin{aligned}
\psi_1(\mathbf{r}_\perp) &= A\lambda \int k_\perp dk_\perp \frac{M_{11}(\mathbf{k}_\perp)\left[M_{11}(\mathbf{k}_\perp) - 1\right] - M_{12}^2(\mathbf{k}_\perp)}{\det\left[M(\mathbf{k}_\perp)\right]} J_0(k_\perp r_\perp), \\
\psi_2(\mathbf{r}_\perp) &= A\lambda \int k_\perp dk_\perp \frac{M_{12}(\mathbf{k}_\perp)}{\det\left[M(\mathbf{k}_\perp)\right]} J_0(k_\perp r_\perp).
\end{aligned} \tag{2.11}$$

The constant A can be determined by imposing the electric neutrality condition. Due to this condition, an ion (with charge $Z_\alpha e$ and diameter D) at the origin is neutralized by its ionic cloud. Thus we have

$$-Z_\alpha e = \int_{r>D} d\mathbf{r}\, \rho(\mathbf{r}). \tag{2.12}$$

Note the above integral runs from $r = D$ to infinity. When combined with Eq. 2.5, Eq. 2.12 becomes

$$\begin{aligned} Z_\alpha e &= \frac{\epsilon}{2\pi\lambda}\left[\int_{r>D} d\mathbf{r}\, \Psi(\mathbf{r})\delta(z) + \int_{r>D} d\mathbf{r}\, \Psi(\mathbf{r})\delta(z-h)\right] \\ &= \frac{\epsilon}{2\pi\lambda}\left[\int_{r>D} d\mathbf{r}_\perp\, \psi_1(\mathbf{r}_\perp) + \int d\mathbf{r}_\perp\, \psi_2(\mathbf{r}_\perp)\right] \\ &= \frac{\epsilon}{\lambda}\left[\int_D^\infty dr_\perp r_\perp \psi_1(r_\perp) + \int_0^\infty dr_\perp r_\perp \psi_2(r_\perp)\right]. \end{aligned} \tag{2.13}$$

Note that the region $r_\perp < D$ is included in the second integral. The explicit expression for A is given by Eq. $A9$ in the Appendix.

Following the Debye charging process [37, 38], the charge fluctuation contribution to the free energy can be obtained. If we consider ψ_1 as a function of $r_\perp$ and e, i.e., $\psi_1(r_\perp, e)$, then the electrostatic free energy of each plate per unit area is given as the following integral:

$$\frac{\mathcal{F}}{k_B T} = \frac{1}{2\pi}\left(\frac{\epsilon}{\lambda Z_\alpha e}\int_0^1 \frac{d\zeta}{\zeta}\psi_1(D, \zeta e) - \frac{1}{2D\lambda}\right). \tag{2.14}$$

Note that ψ_1 incorporate both inter-plate and in-plane charge correlations and is h-dependent (see Eq. $A10$ for explicit expression). The free energy in Eq. 2.14 enables us to systematically study the effect of ionic sizes on the electrostatic attraction between the two plates.

As $D \to 0$, our approach reproduces the known result for point charges [23]. This can be seen by requiring $D = 0$ in Eq. $A10$. Thus the expression for $\psi_1(r_\perp)$ has a simpler

form,

$$\psi_1(r_\perp) = \frac{Z_\alpha e\lambda}{\epsilon}\int_0^\infty k_\perp dk_\perp \frac{M_{11}(\mathbf{k}_\perp)\left[M_{11}(\mathbf{k}_\perp)-1\right]-M_{12}^2(\mathbf{k}_\perp)}{\det\left[M(\mathbf{k}_\perp)\right]} J_0(k_\perp r_\perp). \tag{2.15}$$

The free energy is

$$\begin{aligned}\frac{\mathcal{F}}{k_BT} &= \frac{\epsilon}{2\pi\lambda Z_\alpha e}\int_0^1 \frac{d\zeta}{\zeta}\psi_1(D=0,\zeta e) \\ &= \frac{1}{2\pi}\int_0^1\frac{d\zeta}{\zeta}\int_0^\infty k_\perp dk_\perp \left.\frac{M_{11}(\mathbf{k}_\perp)\left[M_{11}(\mathbf{k}_\perp)-1\right]-M_{12}^2(\mathbf{k}_\perp)}{\det\left[M(\mathbf{k}_\perp)\right]}\right|_{e\to\zeta e}.\end{aligned} \tag{2.16}$$

The ζ-integral in the above equation can be carried out to yield

$$\frac{\mathcal{F}}{k_BT} = \frac{1}{8\pi}\int_0^\infty k_\perp dk_\perp \ln\left\{\det\left[M(\mathbf{k}_\perp)\right]\right\}, \tag{2.17}$$

which is the same as in Ref [23].

2.3 Results and discussions

To study the effect of ionic sizes, we have computed the free energy per unit area with reference to $h=\infty$: $\Delta\mathcal{F} = \mathcal{F}(h) - \mathcal{F}(h=\infty)$. Fig. 2.1 shows $\Delta\mathcal{F}$ (in units of k_BT) as a function of the separation h for different values of the diameter D. We have chosen the parameters $T = 300$K, $\epsilon = 80$ (hence $\ell_B = 7.1$Å), and $\lambda = 1$Å (typical value for DNA or fully charged bilayers). Ionic sizes have non-trivial effects on $\Delta\mathcal{F}$: For $h \gtrsim 5$, $\Delta\mathcal{F}$ gets more negative as D increases. A plausible reason for this is that larger D results in a larger charge polarity–the charge distribution is more heterogeneous–and hence an enhanced attraction. To understand this more clearly, consider a backbone charge on one of the plates (assumed to be at the origin) and its ionic cloud of thickness $\sim \lambda$. Beyond the length scale $\sim D+\lambda$, this plate will appear to be overall neutral to charges on the other plate. Accordingly, this charge (surrounded by the ionic cloud) can be more sensitively felt by counterions on the other plate if D is larger. This may account for

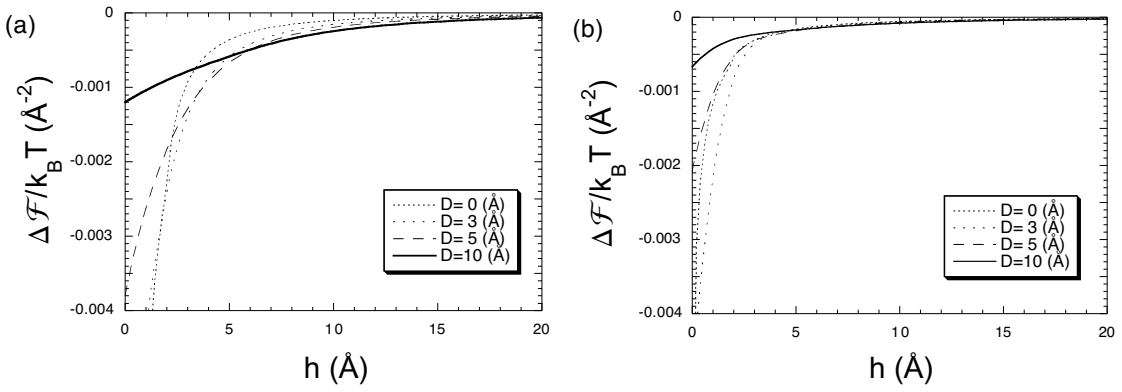

Figure 2.1: The electrostatic free energy of each plate per unit area, $\Delta\mathcal{F}$, as a function of separations h for various choices of D. We have chosen $T = 300$K, $\epsilon = 80$, and $\lambda = 1$Å. For $h \gtrsim 5$Å, the free energy gets more negative as the ion size D increases. For $\lambda = 5$Å (see the inset), however, $\Delta\mathcal{F}$ is less sensitive to D as long as $h \gtrsim 5$Å. As $h \to 0$, however, $\Delta\mathcal{F}$ in both cases remains finite as long as $D > 0$ and is less attractive for larger D.

a stronger attraction between the plates for larger D. (Similar arguments based on a zero-temperature picture can be found in Ref. [27].)

On the other hand, for smaller h, larger D implies a weaker attraction. At first glance, this is somewhat puzzling. As it turns out, small-h behavior reflects single-plate properties. As $h \to 0$, the two plate system resembles a single plate with a surface charge density twice that of each plate: $\Delta\mathcal{F}(\sigma, h \approx 0) \approx \mathcal{F}_1(2\sigma) - 2\mathcal{F}_1(\sigma)$, where $\mathcal{F}_1(\sigma) \equiv \mathcal{F}(\sigma, h = \infty)$ is the corresponding free energy of each plate [37]. For point charges, $\mathcal{F}_1$ diverges (opposite charges can get arbitrarily close to each other). We find that, for $D \ll \lambda$, $\lim_{h\to 0} \Delta\mathcal{F} \to -(k_BT/4\pi\lambda^2)\log(\frac{\lambda}{D})$. For $D \gg \lambda$, however, $\lim_{h\to 0} \Delta\mathcal{F}(h) \to -\left(k_BT/4\pi D^2\right)\log(\frac{D}{\lambda})$. This analysis implies that $|\Delta\mathcal{F}(h \approx 0)|$ decreases as D increases and remains finite as long as $D > 0$, consistent with our results in Fig. 2.1.

For the more weakly charged case of $\lambda = 5$Å (see the inset), however, $\Delta\mathcal{F}$ is almost *in*sensitive to D for large h, i.e. $h \gtrsim 5$Å. On the other hand, for $h \lesssim 5$Å, the effect of

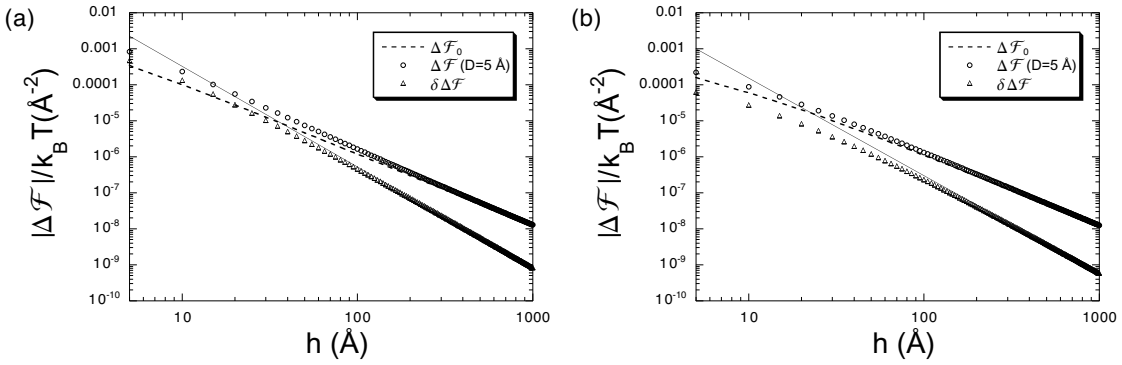

Figure 2.2: Log-log plot of $\Delta\mathcal{F}$, i.e., the electrostatic free energy of each plate per unit area as a function of separations h, for (a) $\lambda = 1$Å and (b) $\lambda = 5$Å. We have chosen $T = 300$K and $\epsilon = 80$. (a) The free energy curve for $D = 0$ ($\Delta\mathcal{F}_0$) is a straight line with a slope 2, confirming the known universal result: $\Delta\mathcal{F}_\infty \sim -k_BT/h^2$. The free energy curve for $D = 5$Å is no longer a straight line, indicating the existence of multiple scaling regimes: The slope of $\delta\Delta\mathcal{F} \equiv \Delta\mathcal{F}(D = 5\text{Å}) - \Delta\mathcal{F}_0$ approaches $s \approx 2.9$ as $h \to \infty$. Our analysis suggests that the free energy is dominated by $\delta\Delta\mathcal{F} \sim 1/h^s$ for $h \lesssim h_{cr} \approx 40$Å and crosses over to $\Delta\mathcal{F}_\infty$ at $h \approx h_{cr}$. (b) For a larger $\lambda = 5$Å, the crossover takes place at a smaller value of h: $h_{cr} \approx 20$Å. Note that the free energy for $D = 0$ in this case is essentially the same as in the previous case (a) for $h \gg \lambda$, as expected.

nonzero D becomes more pronounced; $|\Delta\mathcal{F}(h < 5\text{Å}; D > 0)|$ is smaller for larger D, as in the case of $\lambda = 1$Å.

To study the h dependence of the free energy (per area-plate), i.e., $\Delta\mathcal{F}$, we have displayed $|\Delta\mathcal{F}|$ in units of k_BT as a function of h in a log-log plot, for two different choices of D (see Fig. 2.2): $D = 0$ (dashed line) and $D = 5$Å (circles). We have chosen $T = 300$K and $\epsilon = 80$. Fig. 2.2 (a) and (b) correspond to $\lambda = 1$Å and $\lambda = 5$Å, respectively. First consider the case $\lambda = 1$Å in (a). In this case, the free energy for $D = 0$, $\Delta\mathcal{F}_0 \equiv \Delta\mathcal{F}(D = 0)$, essentially follows the universal scaling behavior, $\Delta\mathcal{F}_\infty \sim -1/h^2$.

The $D = 0$ curve is essentially a straight line with a slope of about 2 throughout the entire range of the plot ($h \geq 5$Å). On the other hand, the h-dependence of $\Delta\mathcal{F}$ for $D = 5$Å is more complicated. The free energy is no longer a straight line in the log-log plot, indicating the existence of multiple scaling regimes. To analyze this case, we plot the difference $\delta\Delta\mathcal{F} \equiv \Delta\mathcal{F}(D = 5\text{Å}) - \Delta\mathcal{F}_0$ (triangles). The $1/h^2$ dependence has been subtracted and the resulting $\delta\Delta\mathcal{F}$ should reflect ion sizes (and charge densities)—$\delta\Delta\mathcal{F}$ depends on D (and λ). The slope of this curve s becomes steeper as h increases and thus does not assume a simple scaling form. It, however, eventually becomes a constant $s \approx 2.9$ as $h \to 1000$Å. This implies that, for large h, $\Delta\mathcal{F} \sim \Delta\mathcal{F}_\infty + a_3/h^s$, where a_3 is the coefficient of the $1/h^s$ term. This large h behavior is consistent with Ref. [20] in which it was shown that $\Pi - \Pi_\infty \sim -A_4/h^4$ in the limit of $h \to \infty$, where λ and D dependence is implicitly included through the coefficient A_4. In this expansion or our our free energy expansion, the term depending on D (and λ) decays faster than $\Delta\mathcal{F}_\infty$. To understand this, first recall that long-wavelength fluctuations lead to a long-ranged interaction; if $\Delta\mathcal{F}_\infty$ arises from $k_\perp \simeq 0$, then higher order terms come from higher $k_\perp$. In light of this, it is not surprising that $\Delta\mathcal{F}_\infty$ does not reflect λ or D dependence, which should be washed out at large-length scales (see also Ref. [20]). A straight line tangent to this curve at large h ($h = 1000$Å) intersects the $D = 0$ curve at $h = h_{cr} \approx 40$Å. This implies that the crossover from $1/h^2$ to $1/h^s$ takes place at $h = h_{cr}$. For $h < h_{cr}$, the free energy decays as $1/h^s$. Beyond this separation, however, it is dominated by $\Delta\mathcal{F}_\infty$.

Fig. 2.2(b) shows the corresponding results for $\lambda = 5$Å. First note that, for $h \gg 5$Å, the $D = 0$ curve ($\Delta\mathcal{F}_0$) is essentially the same as in the case $\lambda = 1$Å; $\Delta\mathcal{F}_0$ for $h \gg \lambda$ follows a universal scaling law [20, 23]. The main difference between the cases ($\lambda = 5$Å and $\lambda = 1$Å) is through the D-dependent term $\delta\Delta\mathcal{F} \sim 1/h^s$ and is two fold: For the larger λ, the free energy is less negative and the crossover takes place at a smaller separation ($h_{cr} \approx 20$Å). Consequently, the effect of nonzero ionic sizes becomes more pronounced

for more highly charged surface—the prefactor of $\delta\Delta\mathcal{F}$ is larger in magnitude for smaller λ.

In light of our results in Fig. 2.2, we have carried out an asymptotic analysis of the free energy $\Delta\mathcal{F}$ (per area-plate). In this limit $h \gg D \gg \lambda$, we find (in the Appendix)

$$\frac{\Delta\mathcal{F}}{k_BT} \sim -\frac{\zeta(3)}{32\pi}\left[\frac{1}{h^2} + \frac{D}{h^3}\ln\frac{h}{\lambda}\right], \tag{2.18}$$

where $\zeta(n)$ is zeta function with $\zeta(3) \approx 1.202$. The first term is the universal power law $\Delta\mathcal{F}_\infty$. On the other hand, the second term arises from finite ionic sizes and makes the free energy more negative. Strictly speaking, this result is valid in the limit $h \gg D \gg \lambda$. Nevertheless this illustrates the significance of finite ionic sizes: The main effect of finite ionic sizes is to make charge distributions more heterogeneous, leading to a larger charge polarity (hence a stronger attraction). It's worth comparing this with the corresponding expansion for $D = 0$: $\Delta\mathcal{F}_0 \sim -\left(h^{-2} - 2\lambda h^{-3}\right)$. The second term in this equation is distinct from the D-dependent term in Eq. 2.18). If the former is repulsive, the latter is attractive. Along this line, it should be emphasized that the latter is analogous to $\delta\Delta\mathcal{F} \sim -1/h^s$ in Fig. 2.2, in the sense that this makes the attraction stronger and is dominant up to h_{cr}, which is larger for larger σ_0. On the other hand, the $1/h^3$ contribution for $D = 0$ becomes negligible for highly charged cases. Finally our asymptotic result in Eq. 2.18, especially the second term, is valid for $h \gg D \gg \lambda$; $\delta\Delta\mathcal{F}$ approaches this term in this limit. In intermediate regions, the D or λ-dependence of $\delta\Delta\mathcal{F}$ can be more complicated than this implies.

In Fig. 2.3, we present electrostatic pressures (per unit area) Π obtained from a few different approaches: the universal pressure, i.e., $\Pi_\infty \sim -k_BT\zeta(3)/8\pi h^3$ with $\zeta(3) = 1.202...$ and $\zeta(n)$ being the Riemann zeta function (thin solid line), DH theory of point charges [23] (dotted lines), our DH approach for $D > 0$ (thick solid lines), and the hypernetted chain (HNC) approximations (diamonds) adopted from Figure 3 of Ref. [20]. Note that essen-

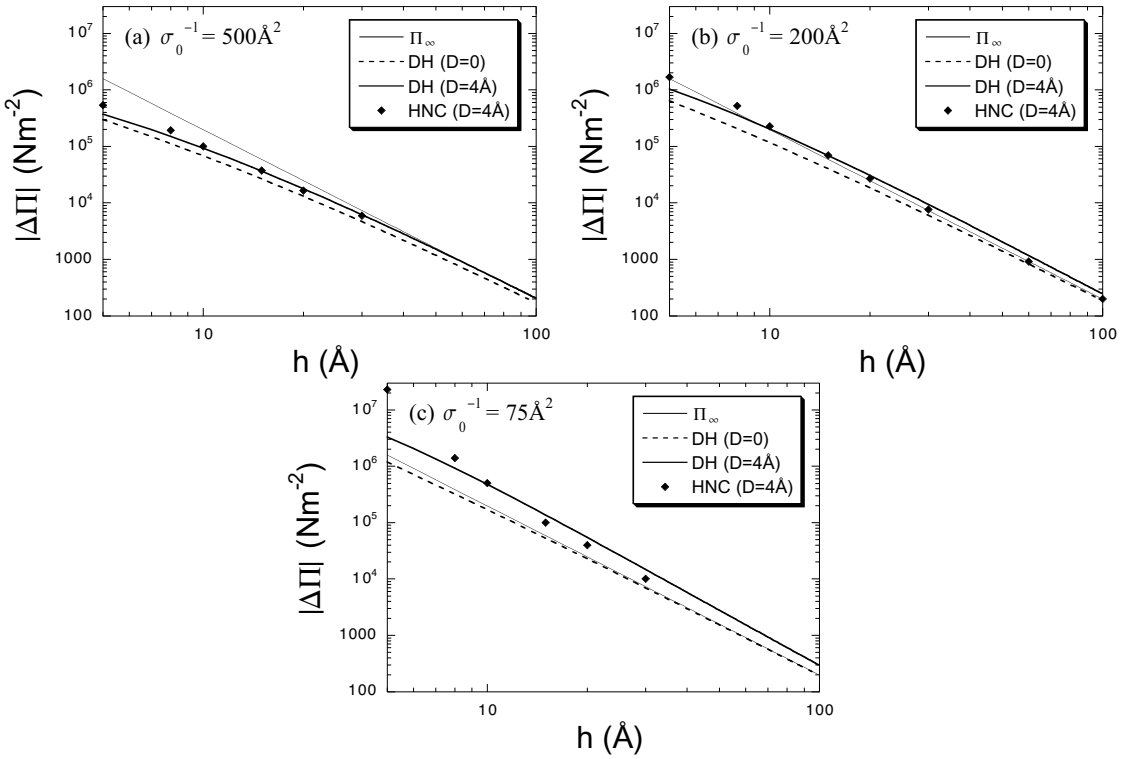

Figure 2.3: Log-log plot of the electrostatic pressure Π per unit area as a function of separations h, for (a) $\sigma_0^{-1} = 500\text{Å}^2$, $Z = 1$, (b) $\sigma_0^{-1} = 200\text{Å}^2$, $Z = 1$, and (c) $\sigma_0^{-1} = 75\text{Å}^2$, $Z = 2$. In all cases, $T = 300\text{K}$ and $\epsilon = 80$. Both our results (DH ($D = 4$Å)) and the hypernetted chain (HNC) approximations for $D = 4$Å from Ref. [20] (diamonds) are more attractive than the corresponding DH results for $D = 0$; the effect of nonzero ionic sizes is more pronounced for larger σ_0. As $h \to \infty$, all these results tend to collapse onto the limiting pressure $\Pi_\infty = \Pi(h \to \infty) \sim -k_B T/h^3$. The agreement between the HNC results and ours is excellent except for Π at $h \simeq 5$Å in (c).

tially the same model was used in the HNC calculations: two overall neutral surfaces carrying mobile cations and anions. In our convention $\Pi = -\partial\left(2\Delta\mathcal{F}\right)/\partial h$. (Recall $\Delta\mathcal{F}$ is the free energy per plate-area.) For our calculations, we have chosen the parameters consistent with Ref. [20]: $D = 4$Å, $T = 300$K, $\epsilon = 80$ (dielectric discontinuity is suppressed in these cases), (a) $\sigma_0^{-1} = 500\text{Å}^2$ and $Z = 1$ ($\lambda = 5.6$Å), (b) $\sigma_0^{-1} = 200\text{Å}^2$ and $Z = 1$ ($\lambda = 2.24$Å), and (c) $\sigma_0^{-1} = 75\text{Å}^2$ and $Z = 2$ ($\lambda = 0.56$Å). In all these cases, both the HNC results and ours are more attractive than the $D = 0$ curves (by several factors at most) for the range shown ($h \geq 5$Å). This clearly suggests that finite ionic sizes enhance the attraction (unless h is too small). For this reason, our results for $D = 4$Å agree better with the HNC results than the $D = 0$ curves. The agreement is excellent for $h \gtrsim 5$Å in (a) and (b). The discrepancy between ours and the HNC result for $\sigma_0^{-1} = 75\text{Å}^2$ at small separations can be attributed to the appearance of a short-rage pressure in the later, which our DH approach suppressed. But note that, in a bilayer system at room temperature, this high density is only realized when the bilayer is fully charged. As h increases, all these results tend to collapse onto the asymptotic pressure as they should. The results in the figure also show how $D = 0$ curves approach the universal pressure Π_∞ as σ_0 increases. Also Π_∞ appears to be favorably compared with both our result and the HNC result for $\sigma_0^{-1} = 200\text{Å}^2$. But this is a coincidence; if we chose larger values of D, then both ours and the HNC results would predict more attractive pressures, while Π_∞ remains the same.

To further study the consequence of finite ionic sizes, we plot, in Fig. 2.4, the free energy per unit area $\Delta\mathcal{F}$ (in units of k_BT) as a function of λ. We have chosen $h = 10$Å, $T = 300$K, and $\epsilon = 80$. As shown in the figure, $\Delta\mathcal{F}$ is sensitive to λ and is more attractive for small λ (corresponding to high σ_0 or Z). These results are consistent with numerical data [35, 36] but deviate from the corresponding results for point charges (the dotted line), which is roughly independent of λ. The results for point charges are somewhat

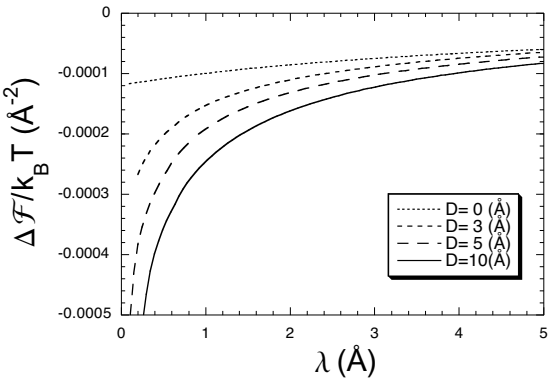

Figure 2.4: The electrostatic free energy per unit area (in units of k_BT) as a function of λ. We have chosen $h = 10$Å, $T = 300$K, and $\epsilon = 80$. As shown in the figure, $\Delta\mathcal{F}$ is sensitive to λ and is more attractive for small λ (corresponding to highly charged case).

different from λ-independent $\Delta\mathcal{F}_\infty$; the latter is simply the large h limit of the former. Note here that the difference between the $D = 0$ pressure and the results for $D \neq 0$ in Fig. 2.4 solely comes from nonzero ionic sizes, since the two are otherwise identical. This is intriguing since it implies that short-length scale properties, i.e., ionic sizes, qualitatively modify λ dependence of $\Delta\mathcal{F}$ (unless h/λ is too large). For $D = 0$, the asymptotic limit, characterized by Π_∞, is realized if $h \gg \lambda$. Our results in Fig. 2.2, however, indicate that for $D > 0$ a new length scale comes: h_{cr}, which is typically much larger than D (see the relevant discussion around Fig. 2.2). In this case, the asymptotic region is reduced down to $h \gg h_{cr}$. For $h \lesssim h_{cr}$, the electrostatic pressure is sensitive to λ as evidenced in Fig. 2.4; it is more sensitive to λ and larger in magnitude for larger D (for $h = 10$Å).

Our DH approach amounts to keeping charge fluctuations at the Gaussian level, leaving out strong charge fluctuations at short length scales as implied by oscillatory charge correlations at low temperatures [31]. In a linearized approach, some of this effect can be, in principle, incorporated by allowing the formation of ion pairs between backbone charges and counterions as much the same way as in the two state model for counteri-

ons. Moreover, it has been shown that out-of-plane charge fluctuations are important and thus the two-dimensional DH approach inevitably underestimates the negative pressure [24,34]. In this regard, the spatial distribution of counterions will further complicate Π. Hence further consideration is certainly warranted. Nevertheless our results can be used to check the self-consistency of our DH approach *within* the two-state model of counterions. In the case of physical interest i.e., $h \gtrsim D \simeq$ 5-10Å, the magnitude of the h-dependent correlation energy is smaller than k_BT. In that case, the DH approach ought to be good. The agreement of our results with those adopted from Ref. [20] is hence not accidental.

2.4 Conclusion

We have developed a theoretical formalism to account for the interplay between ionic sizes and the electrostatic attraction between like charged bilayers. To this end, we have modeled ions (both lipid charges and condensed counterions) as charged hard spheres of diameter D as in the restricted primitive model of a simple ionic fluid. Using a (two-dimensional) Debye-Hückel approach to this system, we have examined how nonzero ionic sizes are intertwined with the attraction. The nonzero ionic size can qualitatively modify the attraction. In the case of physical interest ($h \gtrsim$ 5Å), it enhances the attraction. A plausible reason for this is that the in-plane charge distribution becomes more heterogeneous as D increases, resulting in a larger charge polarity and hence an enhanced attraction. Also the attraction gets stronger as the surface charge density (in units of $-e$) σ_0 increases, consistent with known results [20,27,35]. This observation is interesting, as it implies that the ionic size influences σ_0 dependence of the attraction. In other words, these two effects (ionic sizes and σ_0-dependence of the attraction) are coupled to each other—the attraction is more sensitive to σ_0 for larger D. Our results are in accord with

the long-standing observation of enhanced attractions for high charge densities or large valency and also predicts more realistic results for the pressure that remains finite as $h \to 0$. The main advantage of our approach is that it allows us to systematically study the correlation attraction, without relying on additional approximations/assumptions besides linearization that might obscure the essential physics of correlation attractions.

2.5 Appendix

In this appendix, we present an asymptotic result for the free energy (per plate-area), $\Delta\mathcal{F} = \mathcal{F}(h) - \mathcal{F}(h=\infty)$, in the limit of $h \gg D \gg \lambda$. To this end, we first write $\psi_1(r_\perp)$ explicitly as an integral with respect to $k_\perp$; if we define

$$\overline{\psi}_1(\mathbf{r}_\perp) = \int k_\perp dk_\perp \frac{M_{11}(\mathbf{k}_\perp)\left[M_{11}(\mathbf{k}_\perp)-1\right] - M_{12}^2(\mathbf{k}_\perp)}{\det\left[M(\mathbf{k}_\perp)\right]} J_0(k_\perp r_\perp),$$

$$\overline{\psi}_2(\mathbf{r}_\perp) = \int k_\perp dk_\perp \frac{M_{12}(\mathbf{k}_\perp)}{\det\left[M(\mathbf{k}_\perp)\right]} J_0(k_\perp r_\perp), \qquad (A1)$$

we have

$$\psi_1(\mathbf{r}_\perp) = A\lambda\overline{\psi}_1(\mathbf{r}_\perp),$$

$$\psi_2(\mathbf{r}_\perp) = A\lambda\overline{\psi}_2(\mathbf{r}_\perp). \qquad (A2)$$

The constant A, as determined by Eq. 2.13, is

$$A = \frac{Z_\alpha e}{\epsilon} \frac{1}{\int_D^\infty dr_\perp r_\perp \overline{\psi}_1(r_\perp) + \int_0^\infty dr_\perp r_\perp \overline{\psi}_2(r_\perp)}. \qquad (A3)$$

To carry out the r-integrals in the denominator, we note

$$\begin{aligned} & \int_D^\infty dr_\perp r_\perp \overline{\psi}_1(r_\perp) + \int_0^\infty dr_\perp r_\perp \overline{\psi}_2(r_\perp) \\ = & -\int_0^D dr_\perp r_\perp \overline{\psi}_1(r_\perp) + \int_0^\infty dr_\perp r_\perp \overline{\psi}_1(r_\perp) + \int_0^\infty dr_\perp r_\perp \overline{\psi}_2(r_\perp) \\ = & \int_0^\infty dr_\perp r_\perp \left[\overline{\psi}_1(r_\perp) + \overline{\psi}_2(r_\perp)\right] - \int_0^D dr_\perp r_\perp \overline{\psi}_1(r_\perp). \end{aligned} \qquad (A4)$$

Using this relation [41]

$$\int_0^\infty J_0(k_\perp r_\perp) r_\perp dr_\perp = \frac{\delta(k_\perp)}{k_\perp}, \tag{A5}$$

where $\delta(x)$ is the Dirac δ function, we can simplify the first integral in Eq. A4 as

$$\begin{aligned} & \int_0^\infty dr_\perp r_\perp \left[\overline{\psi}_1(r_\perp) + \overline{\psi}_2(r_\perp)\right] \\ = & \int_0^\infty dk_\perp \delta(k_\perp) \left[1 - \frac{1}{M_{11}(\mathbf{k}_\perp) + M_{12}(\mathbf{k}_\perp)}\right] \\ = & \ 1. \end{aligned} \tag{A6}$$

If we note

$$\int_0^D dr_\perp r_\perp k_\perp J_0(k_\perp r_\perp) = D J_1(k_\perp D), \tag{A7}$$

where $J_1(x)$ is the first-order Bessel function of the first kind, we can rewrite the second integral in Eq. A4 as

$$\int_0^D dr_\perp r_\perp \overline{\psi}_1(r_\perp) = D \int_0^\infty dk_\perp \frac{M_{11}(\mathbf{k}_\perp)\left[M_{11}(\mathbf{k}_\perp) - 1\right] - M_{12}^2(\mathbf{k}_\perp)}{\det\left[M(\mathbf{k}_\perp)\right]} J_1(k_\perp D). \tag{A8}$$

If we use Eqs. A6 and A8 in Eq. A3, we have

$$A = \frac{Z_\alpha e}{\epsilon} \frac{1}{1 - D\int_0^\infty dk_\perp \frac{M_{11}(\mathbf{k}_\perp)[M_{11}(\mathbf{k}_\perp)-1] - M_{12}^2(\mathbf{k}_\perp)}{\det[M(\mathbf{k}_\perp)]} J_1(k_\perp D)}. \tag{A9}$$

This, when combined with Eq. 5, leads to

$$\psi_1(r_\perp) = \frac{Z_\alpha e \lambda}{\epsilon} \frac{\int_0^\infty k_\perp dk_\perp \frac{M_{11}(\mathbf{k}_\perp)[M_{11}(\mathbf{k}_\perp)-1] - M_{12}^2(\mathbf{k}_\perp)}{\det[M(\mathbf{k}_\perp)]} J_0(k_\perp r_\perp)}{1 - D\int_0^\infty dk_\perp \frac{M_{11}(\mathbf{k}_\perp)[M_{11}(\mathbf{k}_\perp)-1] - M_{12}^2(\mathbf{k}_\perp)}{\det[M(\mathbf{k}_\perp)]} J_1(k_\perp D)}. \tag{A10}$$

Now $\psi_1(D, \zeta e) = \psi_1(r = D, e)|_{e \to e\zeta}$. Substituting $\psi(D, \zeta e)$ obtained this way into Eq. 2.14, we have

$$\frac{\mathcal{F}}{k_B T} = \frac{1}{2\pi} \left\{ \int_0^1 \frac{d\zeta}{\zeta} \frac{\int_0^\infty k_\perp dk_\perp \left[\frac{M_{11}(\mathbf{k}_\perp)(M_{11}(\mathbf{k}_\perp)-1) - M_{12}^2(\mathbf{k}_\perp)}{\det[M(\mathbf{k}_\perp)]}\right] J_0(k_\perp D)}{1 - D\int_0^\infty dk_\perp \left[\frac{M_{11}(\mathbf{k}_\perp)(M_{11}(\mathbf{k}_\perp)-1) - M_{12}^2(\mathbf{k}_\perp)}{\det[M(\mathbf{k}_\perp)]}\right] J_1(k_\perp D)} \right|_{e \to e\zeta} - \frac{1}{2D\lambda} \right\}. \tag{A11}$$

For later convenience, we rewrite the term in [...] as

$$\left[\frac{M_{11}(\mathbf{k}_\perp)\left[M_{11}(\mathbf{k}_\perp)-1\right]-M_{12}^2(\mathbf{k}_\perp)}{\det\left[M(\mathbf{k}_\perp)\right]}\right]=\frac{1}{1+\lambda k_\perp}-\frac{M_{12}^2(\mathbf{k}_\perp)}{M_{11}(\mathbf{k}_\perp)\det\left[M(\mathbf{k}_\perp)\right]}. \qquad (A12)$$

Note that the first term is h-independent and that the coupling between the two plates enters through $M_{12}(\mathbf{k}_\perp)$—as expected, $M_{12}(\mathbf{k}_\perp)\to 0$ as $h\to\infty$. Eq. A11 becomes

$$\frac{\mathcal{F}}{k_BT}=\frac{1}{2\pi}\left\{\int_0^1\frac{d\zeta}{\zeta}\left.\frac{\int_0^\infty k_\perp dk_\perp\left[\frac{1}{1+\lambda k_\perp}-\frac{M_{12}^2(\mathbf{k}_\perp)}{M_{11}(\mathbf{k}_\perp)\det[M(\mathbf{k}_\perp)]}\right]J_0(k_\perp D)}{1-D\int_0^\infty dk_\perp\left[\frac{1}{1+\lambda k_\perp}-\frac{M_{12}^2(\mathbf{k}_\perp)}{M_{11}(\mathbf{k}_\perp)\det[M(\mathbf{k}_\perp)]}\right]J_1(k_\perp D)}\right|_{e\to e\zeta}-\frac{1}{2D\lambda}\right\}. \qquad (A13)$$

Following Ref. [37], we find

$$\int_0^\infty k_\perp dk_\perp\frac{1}{1+\lambda k_\perp/\zeta^2}J_0(k_\perp D)=\frac{\zeta^2}{\lambda D}\tau_0\left(\frac{D}{\lambda}\zeta^2\right), \qquad (A14)$$

$$1-D\int_0^\infty dk_\perp\frac{1}{1+\lambda k_\perp/\zeta^2}J_1(k_\perp D)=-\frac{D\zeta^2}{\lambda}\tau_1\left(\frac{D}{\lambda}\zeta^2\right), \qquad (A15)$$

where

$$\tau_n(x)=1-\frac{\pi x^{1-n}}{2}\left[H_n(x)-Y_n(x)\right], \qquad (A16)$$

$H_n(x)$ is the Struve function, and $Y_n(x)$ is the Bessel function of the second kind. If we substitute Eqs. A14 and A15 into Eq. A13, we obtain

$$\frac{\mathcal{F}}{k_BT}=\frac{1}{2\pi}\left\{\int_0^1\frac{d\zeta}{\zeta}\frac{\frac{\zeta^2}{\lambda D}\tau_0(\frac{D}{\lambda}\zeta^2)-\int_0^\infty k_\perp dk_\perp\frac{M_{12}^2(\mathbf{k}_\perp)}{M_{11}(\mathbf{k}_\perp)\det[M(\mathbf{k}_\perp)]}J_0(k_\perp D)}{-\frac{D\zeta^2}{\lambda}\tau_1(\frac{D}{\lambda}\zeta^2)+D\int_0^\infty dk_\perp\frac{M_{12}^2(\mathbf{k}_\perp)}{M_{11}(\mathbf{k}_\perp)\det[M(\mathbf{k}_\perp)]}J_1(k_\perp D)}-\frac{1}{2D\lambda}\right\}. \qquad (A17)$$

From this we obtain, $\Delta\mathcal{F}=\mathcal{F}(h)-\mathcal{F}(h=\infty)$,

$$\frac{\Delta\mathcal{F}}{k_BT}=\frac{1}{2\pi}\int_0^1\frac{d\zeta}{\zeta}\left\{\frac{\frac{\zeta^2}{\lambda D}\tau_0(\frac{D}{\lambda}\zeta^2)-\int_0^\infty k_\perp dk_\perp\frac{M_{12}^2(\mathbf{k}_\perp)}{M_{11}(\mathbf{k}_\perp)\det[M(\mathbf{k}_\perp)]}J_0(k_\perp D)}{-\frac{D\zeta^2}{\lambda}\tau_1(\frac{D}{\lambda}\zeta^2)+D\int_0^\infty dk_\perp\frac{M_{12}^2(\mathbf{k}_\perp)}{M_{11}(\mathbf{k}_\perp)\det[M(\mathbf{k}_\perp)]}J_1(k_\perp D)}-\frac{\frac{\zeta^2}{\lambda D}\tau_0(\frac{D}{\lambda}\zeta^2)}{\left(-\frac{D\zeta^2}{\lambda}\right)\tau_1(\frac{D}{\lambda}\zeta^2)}\right\}. \qquad (A18)$$

We find that, if $h\gg\lambda$,

$$\left|D\int_0^\infty dk_\perp\frac{M_{12}^2(\mathbf{k}_\perp)}{M_{11}(\mathbf{k}_\perp)\det\left[M(\mathbf{k}_\perp)\right]}J_1(k_\perp D)\right|\ll\left|\frac{D\zeta^2}{\lambda}\tau_1(\frac{D}{\lambda}\zeta^2)\right|.$$

This allows us to expand the denominator of the first term in Eq. A18 in powers of the ratio $D\int_0^\infty dk_\perp \frac{M_{12}^2(\mathbf{k}_\perp)}{M_{11}(\mathbf{k}_\perp)\det[M(\mathbf{k}_\perp)]} J_1(k_\perp D)/[\frac{D\zeta^2}{\lambda}\tau_1(\frac{D}{\lambda}\zeta^2)]$. To second order in the ratio, we find

$$\frac{\Delta\mathcal{F}}{k_BT} = \frac{1}{2\pi}\int_0^1 \frac{d\zeta}{\zeta} \quad \left\{ \frac{\int_0^\infty k_\perp dk_\perp \frac{M_{12}^2(\mathbf{k}_\perp)}{M_{11}(\mathbf{k}_\perp)\det[M(\mathbf{k}_\perp)]} J_0(k_\perp D)}{\frac{D\zeta^2}{\lambda}\tau_1\left(\frac{D}{\lambda}\zeta^2\right)} \right.$$
$$\left. - \frac{\frac{\zeta^2}{\lambda}\tau_0\left(\frac{D}{\lambda}\zeta^2\right)\int_0^\infty dk_\perp \frac{M_{12}^2(\mathbf{k}_\perp)}{M_{11}(\mathbf{k}_\perp)\det[M(\mathbf{k}_\perp)]} J_1(k_\perp D)}{\left[\frac{D\zeta^2}{\lambda}\tau_1\left(\frac{D}{\lambda}\zeta^2\right)\right]^2} \right\}. \quad (A19)$$

In the limit of $h \gg D$ and $h \gg \lambda$, the ζ-integral in Eq. A19 is mainly determined by $\zeta \sim \sqrt{\lambda/h}$, which is close to 0. In other words, the main contribution comes from $D\zeta^2/\lambda \sim D/h \ll 1$. This allows us to use the small x expansions of the two functions, $\tau_0(x)$ and $\tau_1(x)$:

$$\begin{aligned} \tau_0(x) &\sim 1 \\ \tau_1(x) &\sim -\frac{1}{x}. \end{aligned}$$

Accordingly, Eq. A19 becomes

$$\frac{\Delta\mathcal{F}}{k_BT} = \frac{1}{2\pi}\int_0^1 \frac{d\zeta}{\zeta} \quad \left\{ -\int_0^\infty k_\perp dk_\perp \frac{M_{12}^2(\mathbf{k}_\perp)}{M_{11}(\mathbf{k}_\perp)\det\left[M(\mathbf{k}_\perp)\right]} J_0(k_\perp D) \right.$$
$$\left. -\frac{\zeta^2}{\lambda}\int_0^\infty dk_\perp \frac{M_{12}^2(\mathbf{k}_\perp)}{M_{11}(\mathbf{k}_\perp)\det\left[M(\mathbf{k}_\perp)\right]} J_1(k_\perp D) \right\}. \quad (A20)$$

The ζ-integral in this equation can be carried out without further approximations:

$$\begin{aligned} \frac{\Delta\mathcal{F}}{k_BT} = \frac{1}{8\pi} & \int_0^\infty k_\perp dk_\perp \ln\left[1 - \frac{\mathrm{e}^{-2hk_\perp}}{(1+\lambda k_\perp)^2}\right] J_0(k_\perp D) \\ +\frac{1}{8\pi} & \int_0^\infty dk_\perp \frac{k_\perp J_1(k_\perp D)}{1-\mathrm{e}^{2hk_\perp}} \left\{ \mathrm{e}^{2hk_\perp} \ln\left[1 - \frac{\mathrm{e}^{-2hk_\perp}}{(1+\lambda k_\perp)^2}\right] \right. \\ & \left. + \mathrm{e}^{hk_\perp} \ln\left[\frac{\mathrm{e}^{hk_\perp}(1+\lambda k_\perp)-1}{\mathrm{e}^{hk_\perp}(1+\lambda k_\perp)+1}\right] + 2\ln\left(1+\frac{1}{\lambda k_\perp}\right) \right\}. \quad (A21) \end{aligned}$$

The free energy can now be expanded in powers of $1/h$. The lowest term scales as $1/h^2$ and the coefficient of this, a_2, can be obtained by multiplying $\Delta\mathcal{F}$ by h^2 and taking

the limit of $h \to \infty$. To this end, we substitute $k_\perp = t/h$ in Eq. A21; the first integral can then be calculated as follows

$$\begin{aligned} & \lim_{h\to\infty} h^2 \int_0^\infty k_\perp dk_\perp \ln\left[1 - \frac{\mathrm{e}^{-2hk_\perp}}{(1+\lambda k_\perp)^2}\right] J_0(k_\perp D) \\ = & \lim_{h\to\infty} \int_0^\infty t dt \ln\left[1 - \frac{\mathrm{e}^{-2t}}{(1+\lambda t/h)^2}\right] J_0\left(\frac{Dt}{h}\right) \\ = & \int_0^\infty t dt \ln(1-\mathrm{e}^{-2t}) \\ = & -\frac{\zeta(3)}{4}. \end{aligned} \qquad (A22)$$

Similarly, we can get a_3, the coefficient of the next leading term, by taking $h \to \infty$ in $h^3(\Delta\mathcal{F} - a_2 h^{-2})$. We find, for $h \gg D$ and $h \gg \lambda$,

$$\frac{\Delta\mathcal{F}}{k_B T} \sim -\frac{\zeta(3)}{32\pi}\left[\frac{1}{h^2} - \frac{2\lambda}{h^3} + \frac{D}{h^3}\left(\ln\frac{h}{\lambda} - C\right)\right], \qquad (A23)$$

where $\zeta(n)$ is zeta function with $\zeta(3) \approx 1.202$ and $C = 1.707$. The first term is the universal power law, independent of surface charge densities and ionic sizes. The other two terms are next leading correction to $\Delta\mathcal{F}$. The third term arises from finite ionic sizes. It remains negative and thus makes the pressure more attractive as long as $h/\lambda \gg 1$. For $D/\lambda \gg 1$, this term dominates the second term. In the limit $h \gg D \gg \lambda$, Eq. A23 reduces to Eq. 2.18 used in the main text.

Chapter 3

Bending of lipid bilayers: relaxed area difference

3.1 Introduction

Bending of lipid bilayers involves two distinct types of deformations: in-plane deformation (stretching or compression) and out-of-plane deformation (bending). We can study the bending of a bilayer in terms of the free energy associated with the deformation. The lowest energy state of the bilayer is characterized by its preferred curvature, which is controlled by two parameters: the spontaneous curvature and the relaxed area difference. A monolayer may have a non-zero spontaneous curvature depending upon head groups and chain packing. The spontaneous curvatures of two monolayers determine that of a bilayer, C_0, a parameter that reflects the asymmetry between the two leaflets (monolayers) of a bilayer. Deviation of the curvature from the spontaneous curvature increases the bending energy. On the other hand, each leaflet of a bilayer has a preferred or relaxed area (A_0^{in} or A_0^{out}), determined by both the number of lipid molecules it contains and

the optimal area each lipid occupies. During bending, however, each leaflet can actually take an area (A^{in} or A^{out}) which is, in general, different from A_0^{in} or A_0^{out}. The difference between A^{in} (A^{out}) and A_0^{in} (A_0^{out}) gives rise to a stress in the bilayer and contributes to the compression energy.

The total deformation free energy of the bilayer can be written as [13]

$$\mathcal{F} = \frac{k_b}{2}\int dA[C_1(\mathbf{r})+C_2(\mathbf{r})-2C_0(\mathbf{r})]^2+k_G\int dAC_1(\mathbf{r})C_2(\mathbf{r})+\frac{\overline{k}_b}{2}\frac{\pi}{AD^2}(\Delta A-\Delta A_0)^2, \quad (3.1)$$

where C_1 and C_2 are two principal curvatures, i.e., the maximum and the minimum values of curvatures at position $\mathbf{r}$, C_0 the spontaneous curvature, A the area of the surface with respect to which C_1 and C_2 are defined, D the thickness of the bilayer, $\Delta A = A^{out} - A^{in}$ the area difference, and $\Delta A_0 = A_0^{out} - A_0^{in}$ is the relaxed area difference. The constants k_b is the bending rigidity or bending modulus, the energy cost of deviating from the spontaneous curvature, k_G is the Gaussian bending modulus, and $\overline{k}_b$ is the area compression modulus. These moduli are properties of molecular composition of a membrane and are determined by the interactions between head groups and between tails. The first two terms in Eq. 3.1 are the bending energy. The third term is the area compression energy.

Based on the basic hypothesis of the continuum mechanical approach to bilayer bending [43–45], the preferred curvature of a bilayer can be determined by minimizing the free energy of a bilayer subject to given constraints on volume and area. The preferred curvature is determined by the spontaneous curvature C_0 and the relaxed area difference ΔA_0.

One may ask what factors determine these parameters and how they change in response to other factors. The current work is aimed at understanding electrostatic aspects of bending. In our work, C_0 and ΔA_0 are related to salt concentrations or surface charge densities. We will discuss factors that determine ΔA_0 in this chapter and defer the

discussion on C_0 to next chapter.

Experiments have shown that the asymmetry in composition of a lipid bilayer can induce bending and thus shape transformation [46–50]. For example, a bilayer vesicle usually contains negatively charged lipids in its inner leaflet, while the outer one is neutral. Raising ionic stregth in solution transforms such a vesicle from concave shapes (corresponding to negative curvatures) toward convex shapes (positive curvatures) [47]. Adding a small concentration of multivalent ions, such as La^{3+} or Gd^{3+}, efficiently shrinks the charged inner leaflet and facilitates such shape transformation [48]. Cholesterol, on the other hand, prefers the outer leaflet and tends to promote convex shapes [49]. Different explanations [13, 50–52] to the observed phenomena are based on the bilayer-couple hypothesis [53], which suggests that small changes in the relaxed area difference ΔA_0 between the two leaflets of a bilayer have a noticeable effect on shapes. Any factor leading to expansion of the inner leaflet relative to the outer one (decreasing ΔA_0) produces a tendency to form concave shapes; on the other hand, any factor that expands the outer leaflet relative to the inner one (increasing ΔA_0) favors convex shapes. While it is empirically known how ligand binding influences ΔA_0, a quantitative picture is still lacking.

In this chapter, we shall calculate the relaxed area difference ΔA_0 of an asymmetrically charged bilayer. We study a model system, i.e., a pure bilayer consisting of two mechanically equal monolayers. The area of each monolayer is the sum of the area occupied by each lipid head group in that monolayer. The optimal head group area can be determined by interactions between head groups at lipid-water interface. We find ΔA_0 is controlled by the balance of a few distinct contributions: net charge repulsions, charge correlations and the entropy of counterion release from the bilayer. The entropic effect is dominant for weakly charged surface in the presence of monovalent counterions only and tends to expand the charged inner leaflet, leading to negative ΔA_0. Charge correlations,

on the other hand, tend to shrink the inner leaflet and promote positive ΔA_0. The sign of ΔA_0 is sensitive to counterion valency.

3.2 Interfacial free energy and optimal head group area of a neutral bilayer

The free energy to remove molecules from the bulk and create interface between two coexisting phases is known as the interfacial free energy. For a lipid bilayer, it is contributed by two opposing forces [55]: attractive and repulsive interactions acting at the interface formed by lipids and water. The area occupied by the head group of a lipid at the lipid-water interface of a bilayer is governed by competition between the two forces.

The attractive contribution to the interfacial free energy can be written as γa, where a is the head group area, and γ is the surface tension at water-lipid interface, which ranges [56] from 20 to 50 mJ m^{-2} (i.e., 0.05 to 0.12 k_BT Å^{-2}, where k_B is the Boltzmann constant and T is the temperature). The repulsive contribution can be represented by k/a, the leading term of any repulsive energy expansion in a^{-1}, where k is a constant. The interfacial free energy per lipid of a bilayer is given, to first order in a^{-1}, as [10]

$$f_1 = \gamma a + \frac{k}{a}. \tag{3.2}$$

The free energy is minimized when

$$\left.\frac{\partial f_1}{\partial a}\right|_{a=a_0} = 0, \tag{3.3}$$

where

$$a_0 = \sqrt{\frac{k}{\gamma}} \tag{3.4}$$

is referred to as *optimal head group area*. Now we can combine Eqs. 3.2 and 3.4 to eliminate k and obtain

$$f_1 = 2\gamma a_0 + \frac{\gamma}{a}(a - a_0)^2, \tag{3.5}$$

The interfacial free energy is now expressed in terms of two measurable parameters, γ and a_0.

3.3 Interfacial free energy and optimal head group area of an asymmetrically charged bilayer

Now we consider an asymmetrically charged lipid bilayer immersed in salty solution. In normal conditions, the outer leaflet of the bilayer is electrically neutral, while the inner leaflet has a negative surface charge density $-e\sigma_0$, attracting oppositely charged counterions such as Na^+ and Ca^{2+}. Some of them are adsorbed onto the surface. They will be referred to as condensed counterions. Others are free in bulk solution. We use n_i for concentrations of free counterions and $e\sigma_i$ for the charge density of condensed counterions ($i = 1$ for monovalent and $i = 2$ for Z-valent counterions). The effective surface charge density of the inner leaflet is

$$-e\sigma^* = -e(\sigma_0 - \sigma_1 - Z\sigma_2). \tag{3.6}$$

The interaction between surface charge and condensed counterions results in an additional term, f_2, in the interfacial free energy. The free energy per lipid of the inner leaflet, f, is now the sum of f_1 and f_2.

$$f = f_1 + f_2 \tag{3.7}$$

Accordingly, the optimal area per lipid that minimizes the free energy shifts to a new value, a_0^*. To find this value, we require

$$\left.\frac{\partial f}{\partial a}\right|_{a=a_0^*} = 0. \tag{3.8}$$

This is equivalent to

$$\left.\frac{\partial f_1}{\partial a}\right|_{a=a_0^*} + \left.\frac{\partial f_2}{\partial a}\right|_{a=a_0^*} = 0. \tag{3.9}$$

The optimal head group area a_0^* can be found by solving Eq. 3.9. To this end, we need to express f_1 and f_2 in terms of a. Although f_1 is given explicitly as a function of a in Eq. 3.5, the expression for f_2 is not so straightforward to obtain.

A previous result [57] gave f_2 as a function of σ_0,

$$f_2 = f_2(\sigma_0), \tag{3.10}$$

and

$$\begin{aligned} -\frac{\partial f_2}{\partial a} &= \Delta\Pi \\ &= \Pi_{ent} + \Pi_{rep} + \Pi_{corr}, \end{aligned} \tag{3.11}$$

where $\Delta\Pi$ is the interfacial tension at the charged surface, and Π_{ent}, Π_{rep} and Π_{corr} are contributions to $\Delta\Pi$ from entropy, electrostatic repulsion, and charge correlations respectively.

As the inner leaflet expands its area, its surface charge density is reduced and some condensed counterions are released to the solution. This process is favored by entropy. The entropy of counterion release tends to expand the area of the inner leaflet. This contribution to $\Delta\Pi$ is given as

$$\beta\Pi_{ent} = \sum_{i=1}^{2} \left[\sigma_i + \left(a \left| \frac{\partial \sigma_i}{\partial a} \right| - \sigma_i \right) \ln \left(\frac{\sigma_i a_c}{n_i v_c} \right) \right]. \tag{3.12}$$

where $\beta = 1/k_B T$, $v_c = 4\pi r_c^3/3$, $a_c = 4\pi r_c^2$ and r_c is the size of counterions.

The repulsive contribution arise from screened repulsion between surface charges and can be written as

$$\beta\Pi_{rep} = -\pi \ell_B \sigma^{*2} \kappa^{-1} - 2\pi \ell_B \kappa^{-1} \sigma^* a \left(\frac{\partial \sigma^*}{\partial a} \right), \tag{3.13}$$

where $\ell_B = e^2/\epsilon k_B T$ is the Bjerrum length, ϵ is the dielectric constant of water and κ^{-1} is the Debye screening length given by $\kappa^2 = 4\pi\ell_B [2n_1 + Zn_2(Z+1)]$. It can be positive for weakly charged surfaces at low salt limit [57].

The charge correlations between surface charges and counterions tend to shrink the inner leaflet and is given as

$$\beta\Pi_{corr} = \frac{1}{4\pi}\int_0^\infty k_\perp dk_\perp \frac{\partial}{\partial a}\left\{ a\left[\ln\left(1+\frac{1}{\lambda\sqrt{k_\perp^2+\kappa^2}}\right)-\frac{1}{\lambda\sqrt{k_\perp^2+\kappa^2}}\right]\right\}, \tag{3.14}$$

where $\lambda^{-1} = 2\pi\ell_B(\sigma_0+\sigma_1+Z^2\sigma_2)$, and correlations are captured at the Gaussian level [23, 31].

The values of σ_i is found by equating the chemical potential of the free counterions, μ_i^{free}, and that of condensed counterions, μ_i^{cond}, where

$$\beta\mu_i^{free} \simeq \ln(n_i v_c), \tag{3.15}$$

$$\beta\mu_i^{cond} \simeq -2\pi Z_i\ell_B\sigma^*\kappa^{-1} + \ln(\sigma_i a_c) + \beta\mu_i^{corr}. \tag{3.16}$$

The first term in Eq. 3.16 arises from the electrostatic interaction between counterions and surface charges, and the second term from the entropy of condensed counterions. The last term, μ_i^{corr}, is the contribution from charge correlations at the Gaussian level:

$$\beta\mu_i^{corr} = \frac{1}{4\pi}\int_0^\infty k_\perp dk_\perp \frac{\partial}{\partial\sigma_i}\left[\ln\left(1+\frac{1}{\lambda\sqrt{k_\perp^2+\kappa^2}}\right)-\frac{1}{\lambda\sqrt{k_\perp^2+\kappa^2}}\right]. \tag{3.17}$$

Since σ_0 changes with a, it proves useful to express f_2 for fixed charge fraction α, the ratio of the number of charged lipids to the total number of lipid. We have

$$\sigma_0 = \frac{\alpha}{a}, \tag{3.18}$$

and

$$f_2 = f_2(a), \tag{3.19}$$

$$-\frac{\partial f_2}{\partial a} = \Delta\Pi(a). \tag{3.20}$$

Hence Eq. 3.9 becomes

$$\Delta\Pi(a_0^*) = \frac{\gamma}{a_0^{*2}}(a_0^{*2} - {a_0}^2). \tag{3.21}$$

Thus a_0^* can be obtained by solving Eq. 3.21 numerically for given α. The change of the optimal head group area of the inner leaflet is

$$\Delta a_0^{in} = a_0^* - a_0. \tag{3.22}$$

3.4 A mean-field result for optimal head group area

While it is hard to solve Eq. 3.21 analytically, a simple expression for a_0^* is possible if we treat the problem in a mean field level. In other words, we ignore correlation contributions, Π_{corr} and μ_i^{corr}.

Now we consider the case of a highly charged surface with a low concentration of monovalent ions ($\kappa\lambda \ll 1$). As surface charges are not effectively screened, the electrostatic interaction dominates the entropy of condensed counterions [58] such that

$$\beta\mu_1^{cond} \simeq -2\pi\ell_B\sigma^*\kappa^{-1}. \tag{3.23}$$

The equilibrium condition now requires

$$\ln(n_1 v_c) \simeq -2\pi\ell_B\sigma^*\kappa^{-1}. \tag{3.24}$$

One can easily find that the effective charge density is approximated by,

$$\sigma^* \simeq -\frac{\kappa \ln(n_1 v_c)}{2\pi\ell_B}, \tag{3.25}$$

which is roughly independent of σ_0 and a. This results in a simpler expression for Π_{rep} and Π_{ent}:

$$\beta\Pi_{rep} \simeq -\pi\ell_B\sigma^{*2}\kappa^{-1}, \tag{3.26}$$

$$\beta\Pi_{ent} \simeq -\sigma^* \ln(n_1 v_c). \tag{3.27}$$

Note the repulsion contribution is negative and shrinks the inner leaflet. We can understand this if we recognize that σ^* is roughly independent of a. Decreasing a results in a lower free energy and is favored by this contribution.

Combining Eqs. 3.25, 3.26, 3.27, we have

$$\begin{aligned} \Delta\Pi &= \Pi_{rep} + \Pi_{ent} \\ &\simeq \frac{k_B T \kappa \left[\ln(n_1 v_c)\right]^2}{4\pi \ell_B}, \end{aligned} \tag{3.28}$$

which is a-independent. From Eq. 3.21, we have

$$a_0^* = a_0 \sqrt{\frac{1}{1-x}}, \tag{3.29}$$

where $x = \Delta\Pi/\gamma$.

The magnitude of $\Delta\Pi$ is on the order of 10^{-3} $k_B T$ Å^{-2} [57]. In contrast, γ lies between 0.05 and 0.1 $k_B T$ Å^{-2}. Thus we can expand Eq. 3.29 for small $x = \Delta\Pi/\gamma$ to obtain

$$a_0^* = a_0 \left[1 + \frac{x}{2} + O(x)\right]. \tag{3.30}$$

The change in optimal head group area per lipid is

$$\begin{aligned} \Delta a_0^{in} &= a_0^* - a_0 \\ &= a_0 \left[\frac{x}{2} + O(x)\right]. \end{aligned} \tag{3.31}$$

3.5 Area difference of a bilayer

In the above discussion, we have obtained the optimal head group area per lipid of an asymmetrically charged bilayer. A typical experimental study of bilayer vesicles records their shape as the surface area is changed. If A_0^{out} is the relaxed area of the outer leaflet of the bilayer and A_0^{in} is that of the inner leaflet, the relaxed area difference due to $\Delta\Pi$ is

$$\Delta A_0 = A_0^{out} - A_0^{in}. \tag{3.32}$$

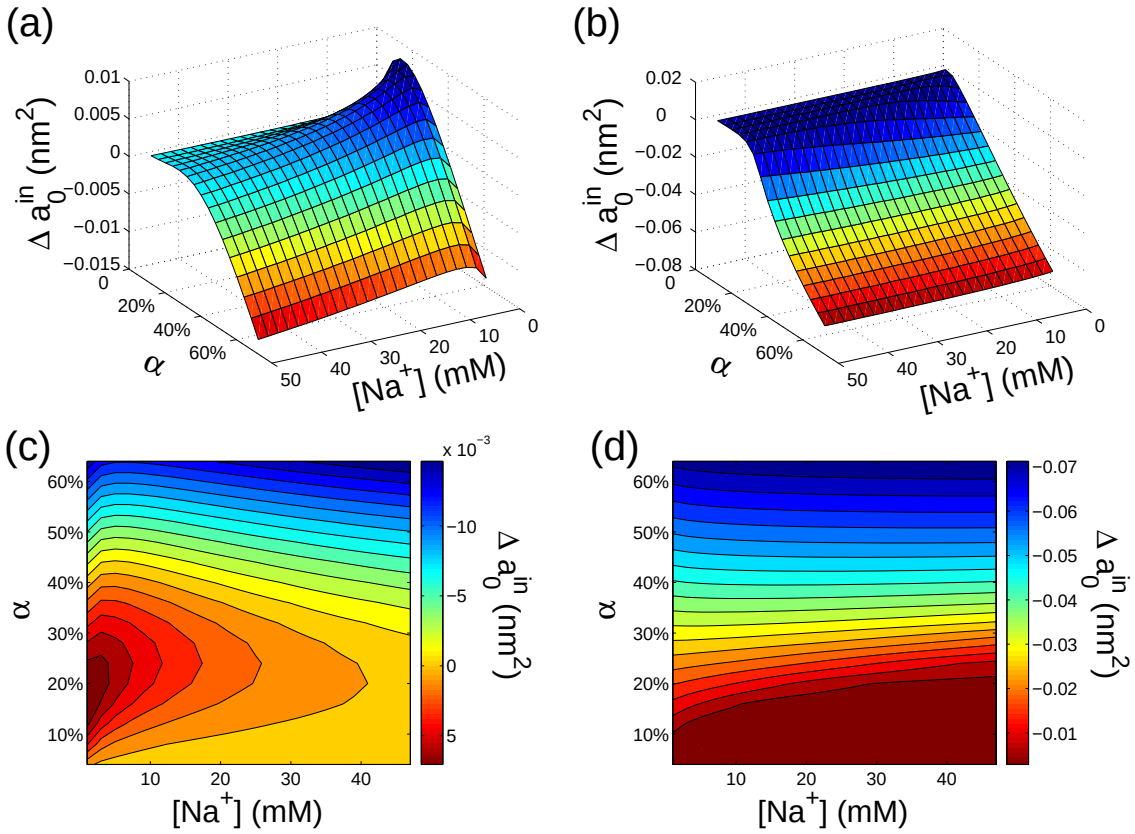

Figure 3.1: Change in relaxed area per lipid in the inner leaflet, Δa_0^{in}, as a function of the sodium concentration in millimole, [Na^+], and the surface charge fraction, α. (a) Three-dimensional plot of Δa_0^{in} in the absence of divalent counterions. (b) Three-dimensional plot of Δa_0^{in} in the presence of 0.1 mM divalent counterions. (c) Contour plot of Δa_0^{in} in the absence of divalent counterions. (d) Contour plot of Δa_0^{in} in the presence of 0.1 mM divalent counterions. The value of Δa_0^{in} is positive for smaller α and [Na^+] in the monovalent case but turns negative as α or [Na^+] increases. In the presence of divalent counterions, Δa_0^{in} is negative for a wide parameter range plotted.

We first discuss how solution conditions modify the relaxed area difference ΔA_0. This can be demonstrated by considering the change in relaxed area per lipid in the inner leaflet, $\Delta a_0^{in} = a_0^* - a_0$. Since the neutral outer leaflet has a constant relaxed area per lipid, a_0, and the two leaflets are identical except for the charge asymmetry, $\Delta A_0 = N(a^{out} - a^{in}) = N(a_0 - a_0^*) = -N\Delta a_0^{in}$, where N is the number of lipids on each leaflet. We have solved Eq. 3.21 and plotted Δa_0^{in} as a function of the concentration of counterions, $[Na^+]$, and the charge fraction, α, in Fig. 3.1. We have chosen the parameters $T = 300$K, $\epsilon = 80$, $r_c = 2$Å and $\gamma = 50$ mJ m^{-2} ($\sim 0.12\ k_BT$). The optimal head group area of a bilayer is usually $50 \sim 100$ Å^2. We thus have chosen $a_0 = 80$Å^2. We find Δa_0 is more sensitive to α or counterion valency but less sensitive to $[Na^+]$: In the absence of divalent counterions, Δa_0^{in} is negative except for weakly charged surfaces at low salt concentrations; in contrast, when the solution contains 0.1 mM divalent counterions, Δa_0^{in} decreases dramatically and remains negative for nearly all parameter range plotted. The difference between two cases can be attributed to the competition of Π_{rep}, Π_{ent}, and Π_{corr}. For small α, Π_{ent} is dominant, leading to positive Δa_0^{in}. For large α, $\Delta\Pi$ is dominated by Π_{corr}, which shrinks the inner leaflet and leads to negative Δa_0^{in}. Note that Π_{rep} is not always positive and can easily be dominated by the other two (see Ref. [57] for details). In the presence of divalent counterions, Π_{corr} is greatly enhanced and counterbalances Π_{ent}, leading to negative Δa_0^{in}.

Besides, Δa_0^{in} changes non-monotonically as a function of $[Na^+]$ for monovalent cases but monotonically in the presence of divalent counterions. This can also be explained in terms of Π_{rep}, Π_{ent}, and Π_{corr}. For small α, Π_{ent} dominates $\Delta\Pi$ and changes non-monotonically with $[Na^+]$ at small $[Na^+]$. This effect is controlled both by $[Na^+]$ and by σ^*. As $[Na^+]$ increases, the entropic effect of counterion release is less significant. On the other hand, $\sigma^* \to 0$ as $[Na^+] \to 0$, since more counterions are condensed (cf. Eq. 3.27). This leads to $\Pi_{ent} \to 0$. The interplay between condensation and counterion release

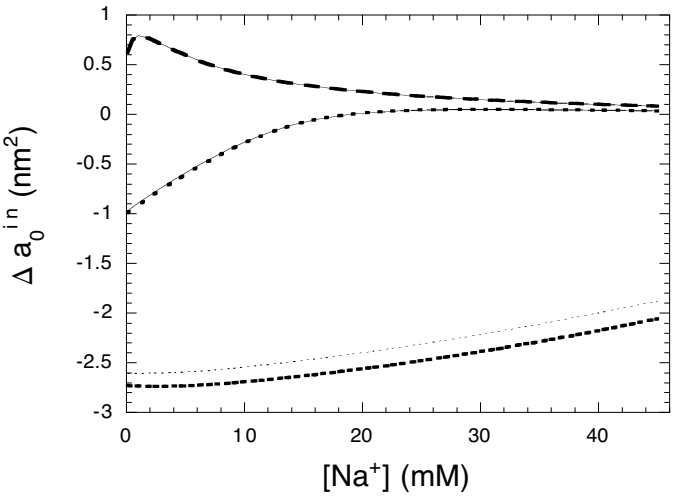

Figure 3.2: Comparison between Δa_0^{in} calculated for fixed charge fraction α and for fixed surface charge density. Thick lines represent Δa_0^{in} for fixed α; thin lines represent Δa_0^{in} for fixed σ_0. Three sets of lines from top to bottom are for $\sigma_0 = 0.2$ nm^{-2} (monovalent counterions), $\sigma_0 = 0.2$ nm^{-2} (0, 1 mM divalent counterions) and $\sigma_0 = 0.38$ nm^{-2} (0, 1 mM divalent counterions), respectively. The corresponding α are 16%, 16% and 30%, respectively. In each of the first two sets, the curve calculated for fixed α overlaps that for fixed σ_0.

gives rise to the non-monotonical behavior of Π_{ent} and consequently that of Δa_0^{in}. In the absence of divalent counterions, the counterion release is more pronounced around $[Na^+] \sim 2$ mM. When 0.1 mM divalent counterions such as Ca^{2+} are presented in the solution, they preferentially bind to the inner leaflet as it reduces energy more efficiently than $[Na^+]$ does. As a result, Π_{corr} is enhanced and dominant over Π_{ent}, making Δa_0^{in} insensitive to $[Na^+]$.

Surface charge density σ_0 is a function of optimal head group area a_0^* and is given by $\sigma_0 = \alpha/a_0^*$. As the inner leaflet with a fixed α expands or compresses its area to relieve stress, σ_0 and $\Delta\Pi$ changes accordingly. Our calculation have included this effect.

However, sometimes we may want to avoid numerical solution to Eq. 3.21. We find it helpful to assume σ_0 is approximately fixed (i.e., $\sigma_0 \simeq \alpha/a_0$), as Δa_0^{in} is relatively small compared to a_0, especially for monovalent cases (Fig. 3.1 (a)) or for weakly charged surfaces in the presence of divalent counterions (Fig. 3.1 (b)). In this case, Eq. 3.21 can be solved analytically, and a_0^* is given by

$$a_0^* = a_0\sqrt{\frac{1}{1-x}}. \tag{3.33}$$

where $x = \Delta\Pi/\gamma$. To test how good this approximation is, we plot the dependence of Δa_0^{in} on [Na^+] for fixed α and for fixed σ_0 in Fig. 3.2. We choose $\sigma_0 = 0.2$ nm^{-2} in the presence of monovalent counterions only, $\sigma_0 = 0.2$ nm^{-2} in the presence of 0.1 mM Ca^{2+}, and $\sigma_0 = 0.38$ nm^{-2} in the presence of 0.1 mM Ca^{2+}. For $a_0 = 80$Å, the corresponding $\alpha = 16\%$, 16% and 30%, respectively (according to $\sigma_0 = \alpha/a_0$). The difference in the first two cases is negligible, as Δa_0^{in} is relatively small for small α. Thus this approximation is valid. For $\alpha = 30\%$ in the presence of divalent counterions, the difference cannot be ignored and our numerical solution is more reliable.

3.6 Conclusion

To summarize, we have developed a formalism for calculating the relaxed area difference of an asymmetrically charged bilayer immersed in salty solution. This relaxed area difference is modified by interactions between surface charges and counterions.

We find the entropic contribution Π_{ent} is dominant for small α at low [Na^+] and is responsible for the positive value and the non-monotonic behavior of Δa_0^{in}. However, Π_{corr} counterbalances Π_{ent} in the presence of divalent counterions and shrinks the inner leaflet, leading to negative Δa_0^{in} roughly independent of [Na^+]. Our results are consistent with experiments that multivalent cations promote positive ΔA_0 and positive curvatures.

In addition to ΔA_0, the preferred curvature of a bilayer is also determined by the spontaneous curvature C_0. In next chapter, we will develop a model to determine C_0 of a bilayer arising from charge asymmetry.

Chapter 4

Bending of lipid bilayers: spontaneous curvature

4.1 Introduction

Two parameters control the preferred curvature of a lipid bilayer: the relaxed area difference ΔA_0 and the spontaneous curvature C_0. In the previous chapter, we have determined ΔA_0 of an asymmetrically charged bilayer. In this chapter, we shall discuss the spontaneous curvature C_0. For an arbitrarily selected reference surface, the deformation free energy of the bilayer generally contains the term ($\sim (\Delta A - \Delta A_0)^2$). If we want to focus on the spontaneous curvature, we need to eliminate this term. To this end, we choose a *neutral surface*, the area of which does not change during bending, for each leaflet of the bilayer. (The existence of such a surface is shown in Chapter 6 of Ref. [59]). With reference to the neutral surface of the inner (outer) leaflet, $A^{in} = A_0^{in}$ ($A^{out} = A_0^{out}$), such that $\Delta A = \Delta A_0$. The deformation free energy of the bilayer thus comes solely from bending energy or curvature energy, i.e., the energy associated with the out-of-plane deformation.

The phenomenological formula for the curvature energy per unit area, f_c, up to quadratic order in the two principal curvatures, c_1 and c_2, can be written as [44]

$$f_c = 2k_b(H - c_0)^2 + k_G K, \tag{4.1}$$

or

$$f_c = \frac{1}{2}k_b(c_1 + c_2 - 2c_0)^2 + k_G c_1 c_2, \tag{4.2}$$

where $H = (c_1 + c_2)/2$ is the mean curvature, $K = c_1 c_2$ is the Gaussian curvature, k_b is the bending rigidity or bending modulus and k_G is the Gaussian bending modulus. The parameter c_0, first introduced by Helfrich [44], is the *spontaneous curvature*, the mean curvature that minimizes the curvature free energy. It describes the tendency of a membrane to bend either inward or outward. For a monolayer, it arises from the packing ratio, a parameter that describes the geommetry of lipids. For example, cone-like lipids can pack into a monolayer with a finite spontaneous curvature; cylindrical-shaped lipids can form a monolayer with $c_0 = 0$. A bilayer may have a spontaneous curvature if there is an asymmetry in the packing ratios of the two constituent leaflets.

The concept of spontaneous curvature can be used to discuss the behavior of bilayers, such as shapes or undulation. In the study of bilayer vesicle shapes, for example, bilayers are treated as a two-dimensional fluid with a bending rigidity and a spontaneous curvature. Vesicle shape is determined by minimizing the curvature free energy of the bilayer. A series of possible axisymmetric vesicle shapes were predicted in this way [45, 60, 61].

The physical origin of the spontaneous curvature is a present interest. For example, it may arise from charge asymmetry between the inner and outer leaflets of a bilayer. The charge properties of both the bilayer and the adjacent solutions may affect the spontaneous curvature. Many theoretical papers on the spontaneous curvature focus on electrostatics of the spontaneous curvature. The electrostatic contributions to the spontaneous curvature was quantified within the Debye-Hückel (DH) approximation for

weakly charged surfaces [6]. Further results for highly charged systems were calculated by solving the nonlinear Poisson-Boltzmann (PB) equation to obtain electrical potentials for cylindrical and spherical geometries. Although full analytical solutions to the nonlinear PB equation are still unknown, the free energy was expanded to quadratic order in curvatures for the aforementioned geometries [62, 63]. This approach has been used for monolayers [63], then for bilayers [64] and for undulating membranes [65]. In a recent paper, Chou et al. [66] calculated electrostatic contributions to spontaneous curvature within both the DH and the PB theories under a variety of assumptions. In particular, they systematically explored the effect of different choices of neutral surface, i.e., the mid-plane of the bilayer or the lipid-water interface. However, all these works on the electrostatic contribution to the spontaneous curvature remain at the mean field level, where charge correlations are suppressed. For a highly charged surface in the presence of multivalent salts, charge correlations can be strong [57] and may influence the spontaneous curvature in a non-trivial way.

In this chapter, we will develop a theory of electrostatics of the spontaneous curvature that captures charge correlations at the Gaussian level. In contrast to the previous Refs. [6, 62–66], our theory is based on a microscopic model for a lipid monolayer [59], in which the spontaneous curvature is determined by the mechanical properties of lipids, e.g., the optimal head group area and the equilibrium length of the hydrocarbon tail. We use the optimal head group area, discussed in the previous chapter, to calculate the spontaneous curvature of an asymmetrically charged bilayer. In this way, we are able to describe the spontaneous curvature in terms of salt concentrations and surface charge fractions of a bilayer. One advantage of our method is that it captures charge correlation contribution to the spontaneous curvature, which can become dominant over entropy and screened electrostatic repulsions under certain conditions; this has been ignored in the previous models [6, 62–66]. As the spontaneous curvature is obtained in terms of local

curvatures, our model is applicable to any geometry in addition to the usually discussed symmetrical ones.

In what follows, we first review the microscopic model for a monolayer and extend it to a bilayer composed of two monolayers. We shall use c_0 for the spontaneous curvature of a monolayer and C_0 for that of a bilayer. We then apply this model to an asymmetrically charged bilayer immersed in salty solution and obtain its spontaneous curvature. In discussion we will compare our theory to the previous ones at the mean-field level.

4.2 Spontaneous curvature of a monolayer

The microscopic model [59] was introduced to describe the spontaneous curvature of a monolayer in terms of a few molecular properties, such as the optimal head group area, the equilibrium chain length, and the chain volume. The hydrocarbon chains in the monolayer are modeled as springs with a spring constant k_s and an equilibrium length l_s. In most systems, changing the volume of a membrane costs higher energy than bending it. Thus a chain in the monolayer is assumed to occupy an incompressible volume v_0 such that this volume is fixed during curvature deformation. Also fixed is the optimal head group area, a_0, which is determined by the interactions between head groups. As these interactions are much stronger than the chain stretching energy, a_0 is not affected by the curvature deformation. In other words, the neutral surface is chosen to be the lipid-water interface.

The free energy per lipid is related to stretch or compression of chains,

$$f = \frac{1}{2}k_s(l - l_s)^2, \tag{4.3}$$

where l is actual chain length. For a flat monolayer, the equilibrium chain length $l_s = v_0/a_0$. In general, v_0/a_0 is unequal to l_s, implying the free energy of a monolayer does

not have to be a minimum. The chains tend to reach their equilibrium length, l_s, while keeping v_0 constant. As a result, the monolayer bends to minimize its free energy. The volume of a chain, v_0, is given in terms of curvatures for a curved monolayer:

$$v_0 = a_0 l \left(1 + lH + \frac{1}{3} l^2 K\right), \tag{4.4}$$

where H and K are mean and Gaussian curvatures respectively . We can determine the curvature free energy f by solving Eq. 4.4 for l in terms of H and K and substitute it into Eq. 4.3. This can be done if we require

$$l = l_0 + l_1 H + l_2 H^2 + l_3 K \tag{4.5}$$

in Eq. 4.4. Thus we have

$$\begin{aligned} l_0 &= \frac{v_0}{a_0}, \qquad l_1 = -l_0^2, \\ l_2 &= 2l_0^2, \qquad l_3 = -\frac{l_0^3}{3}. \end{aligned} \tag{4.6}$$

The curvature free energy per lipid for a monolayer, when $c_0 l_s \ll 1$, is obtained up to second order in curvature as

$$f = \frac{k_s v_0^4}{2a_0^4} \left[(H - c_0)^2 - \frac{2c_0 v_0}{3a_0} K\right]. \tag{4.7}$$

The spontaneous curvature c_0 is determined by the optimal area per molecule a_0, chain volume v_0, and equilibrium chain length l_s:

$$c_0 \;=\; \frac{a_0(v_0 - a_0 l_s)}{v_0^2}. \tag{4.8}$$

If the optimal head group area, a_0, determined by head group interactions, is smaller than the preferred area which minimizes the curvature free energy, v_0/l_s, c_0 is positive and the monolayer has a tendency of bending toward head groups. If $a_0 > v_0/l_s$, c_0 is negative and the monolayer tends to bend toward the chain.

4.3 Spontaneous curvature of a bilayer

For a bilayer composed of two adjacent monolayers, we consider here a simple case. We assume the two monolayers are identical except for their optimal head group area. Each of the monolayers has the same chain volume v_0 and an equilibrium chain length l_s. The bilayer thickness is $D = 2l_s$. The optimal head group areas of the inner and the outer layers are a_0^{in} and a_0^{out}, respectively. We also assume the chains of two layers do not penetrate each other. As a result, there is no interaction between two monolayers that contributes to curvature free energy other than the incompressibility condition: the chain volume of each monolayer is constant. The neutral surface of each monolayer is taken to be its lipid-water interface. Once a_0^{in} and a_0^{out} are given, the spontaneous curvature of the bilayer can be determined.

It is convenient to choose a common reference surface for two leaflets forming a bilayer. To this end, we choose the mid-plane, the interface between two leaflets, as the reference surface throughout this chapter. The curvature free energy per unit area of a bilayer with reference to the mid-plane, $\mathcal{F}$, is simply a sum of the free energies per unit area of the two monolayers:

$$\mathcal{F} = \frac{f^{in}}{a_i^m} + \frac{f^{out}}{a_o^m}, \tag{4.9}$$

where a_i^m (a_o^m) is the area on the mid-plane occupied by a lipid on the inner (outer) leaflet and f^{in} (f^{out}) is the curvature free energy per lipid of the inner (outer) leaflet:

$$f^{in}(H^{in}, K^{in}) = \frac{k_s v_0^4}{2(a_0^{in})^4}\left[(H^{in} - c_0^{in})^2 - \frac{2c_0^{in}v_0}{3a_0^{in}}K^{in}\right], \tag{4.10}$$

$$f^{out}(H^{out}, K^{out}) = \frac{k_s v_0^4}{2(a_0^{out})^4}\left[(H^{out} - c_0^{out})^2 - \frac{2c_0^{out}v_0}{3a_0^{out}}K^{out}\right], \tag{4.11}$$

where H^{in} (H^{out}) and K^{in} (K^{out}) are the mean and the Gaussian curvatures of the inner (outer) leaflet respectively and a_0^{in} (a_0^{out}) is the optimal head group area of the inner (outer) leaflet. As defined in Eq. 4.8, c_0^{in} (c_0^{out}) is the spontaneous curvature of the inner

(outer) monolayer with respect to its neutral surface.

In adding the two free energies, one has to be careful about two things. First, the sign of curvatures of the two monolayers forming a bilayer are always opposite to each other. The sign of curvature for a monolayer has been defined in the preceding discussion such that a positive curvature corresponds to bending toward head groups. Second, the curvatures of the two monolayers are defined with reference to two different surfaces due to the finite thickness of a bilayer. They can be related to each other as the thickness of the bilayer is fixed. If we shift a surface, with mean curvature H and Gaussian curvature K along its normal direction, a distance d to obtain a surface parallel to the original one with curvatures H' and K', we have [59]

$$H' = \frac{H + Kd}{1 + 2Hd + Kd^2}, \tag{4.12}$$

and

$$K' = \frac{K}{1 + 2Hd + Kd^2}. \tag{4.13}$$

If we assume $Hd \ll 1$ and $Kd^2 \ll 1$, we can expand H' and K' in powers of Hd and Kd^2 and keep terms up to second order in curvature:

$$\begin{aligned} H' &\approx (H + Kd)(1 - 2Hd - Kd^2) \\ &\approx H - 2H^2 d + Kd, \end{aligned} \tag{4.14}$$

and

$$\begin{aligned} K' &\approx K(1 - 2Hd - Kd^2) \\ &\approx K. \end{aligned} \tag{4.15}$$

Note higher order terms like H^3, HK or K^2 have been ignored. The relation between the area elements of two surface, δa and $\delta a'$ is

$$\delta a' = (1 + 2Hd + Kd^2)\delta a. \tag{4.16}$$

It is more convenient to express curvatures of both the inner and the outer layers in terms of H^m and K^m, the mean and the Gaussian curvatures with reference to the mid-plane. The sign of H^m is defined such that it is the same as the sign of H^{in}. If we choose

$$\begin{aligned} H' = H^{in}, \qquad & K' = K^{in}, \\ H = H^m, \qquad & K = K^m, \\ d = -\frac{D}{2}, & \end{aligned} \tag{4.17}$$

in Eqs. 4.14 and 4.15, we find

$$H^{in} \approx D(H^m)^2 + H^m - \frac{D}{2}K^m, \tag{4.18}$$

$$K^{in} \approx K^m. \tag{4.19}$$

To express H^{out} and K^{out} in terms of H^m and K^m, we choose

$$\begin{aligned} H' = -H^{out}, \qquad & K' = K^{out}, \\ H = H^m, \qquad & K = K^m, \\ d = \frac{D}{2}. & \end{aligned} \tag{4.20}$$

We find

$$H^{out} \approx D(H^m)^2 - H^m - \frac{D}{2}K^m, \tag{4.21}$$

$$K^{out} \approx K^m. \tag{4.22}$$

Note that the sign of H^{out} is opposite to that of H^{in} and H^m. Similarly, we can express a_i^m (a_o^m) in terms of a^{in} (a^{out}), H^m and K^m,

$$a_i^m = \frac{a_0^{in}}{(1 - H^m D + K^m D^2/4)}, \tag{4.23}$$

$$a_o^m = \frac{a_0^{out}}{(1 + H^m D + K^m D^2/4)}. \tag{4.24}$$

These relations can also be derived by considering symmetric shapes such as a sphere or a cylinder.

Expressed in H^m and K^m, the free energies per lipid for the inner and the outer leaflets are

$$f^{in}(H^m,K^m) = \frac{k_s v_0^4}{2(a_0^{in})^4}\left\{\left[D(H^m)^2+H^m-\frac{D}{2}K^m-c_0^{in}\right]^2-\frac{2c_0^{in}v_0}{3a_0^{in}}K^m\right\} \quad (4.25)$$

$$f^{out}(H^m,K^m) = \frac{k_s v_0^4}{2(a_0^{out})^4}\left\{\left[D(H^m)^2-H^m-\frac{D}{2}K^m-c_0^{out}\right]^2 - \frac{2c_0^{out}v_0}{3a_0^{out}}K^m\right\}. \quad (4.26)$$

Now we can get the curvature free energy of a bilayer as a function of H^m up to second order in curvature:

$$\begin{aligned}\mathcal{F} &= \frac{f^{in}}{a_i^m}+\frac{f^{out}}{a_o^m} \\ &= f_0+f_1H^m+f_2(H^m)^2+f_3K^m. \end{aligned} \quad (4.27)$$

The coefficients f_i are

$$f_0 = \frac{k_s v_0^4}{2}\left[\frac{c_0^{in\,2}}{(a_0^{in})^5}+\frac{c_0^{out\,2}}{(a_0^{out})^5}\right], \quad (4.28)$$

$$f_1 = \frac{k_s v_0^4}{2}\left[\frac{c_0^{out}(2+Dc_0^{out})}{(a_0^{out})^5}-\frac{c_0^{in}(2+Dc_0^{in})}{(a_0^{in})^5}\right], \quad (4.29)$$

$$f_2 = \frac{k_s v_0^4}{2}\left[\frac{1}{(a_0^{in})^5}+\frac{1}{(a_0^{out})^5}\right], \quad (4.30)$$

$$f_3 = \frac{k_s v_0^4}{2}\left[\frac{c_0^{in}}{(a_0^{in})^5}\left(D+\frac{D^2c_0^{in}}{4}-\frac{2v_0}{3a_0^{in}}\right)+\frac{c_0^{out}}{(a_0^{out})^5}\left(D+\frac{D^2c_0^{out}}{4}-\frac{2v_0}{3a_0^{out}}\right)\right] \quad (4.31)$$

We find that the mean curvature at which $\mathcal{F}_{total}$ is minimized,

$$C_0=-\frac{f_1}{2f_2}, \quad (4.32)$$

is the spontaneous curvature with reference to the mid-plane of the bilayer.

4.4 Spontaneous curvature of an asymmetrically charged bilayer

In this section we study the spontaneous curvature of a bilayer containing charged lipids. We consider the case of an asymmetrically charged bilayer in salty solution: The inner leaflet of the bilayer has a surface charge density $-e\sigma_0$, capable of adsorbing counterions, while the outer leaflet is electrically neutral. The two leaflets are otherwise identical—the lipids on each leaflet have the same chain length l_s and volume v_0. Counterions are either condensed or free in solution. We assume that the neutral outer leaflet has an optimal head group area $a_0^{out} = a_0$ and a spontaneous curvature c_0^{out}. As ions will not influence a_0 and thus c_0^{out}, we choose $c_0^{out} = 0$ for simplicity. This implies $v_0/a_0 = l_s$. However, the free energy of the inner leaflet is modified by the interactions between surface charges and counterions. The optimal head group area of the inner leaflet shifts to a new value, $a_0^{in} = a_0^*$, which is a function of salt concentrations and the surface charge densities and has been discussed in the previous chapter. For the inner leaflet, the change in a_0^{in} results in a nonzero spontaneous curvature

$$c_0^{in} = \frac{a_0^*(v_0 - l_s a_0^*)}{v_0^2}. \tag{4.33}$$

This, together with $c_0^{out} = 0$, will determine the spontaneous curvature of the bilayer.

If we apply Eq. 4.32 to the asymmetrically charged bilayer, we obtain the spontaneous curvature with reference to the mid-plane,

$$C_0 = \frac{a_0^5 c_0^{in}(2 + D c_0^{in})}{2[a_0^5 + (a_0^*)^5]}, \tag{4.34}$$

where $D = 2l_s$ is the thickness of the bilayer. The value of a_0^* as a function of salt concentrations can be obtained by solving Eq. 3.21. Note this spontaneous curvature comes solely from electrostatics. If both leaflets were neutral, we would have $c_0^{in} = 0$ and $C_0 = 0$. This means that there is no mechanical contribution to C_0.

4.5 Results and discussions

In this section we investigate the spontaneous curvature of an asymmetrically charged bilayer. This charge asymmetry results in a difference in the optimal head group areas of lipids on the two leaflet , which induces the spontaneous curvature of a bilayer. Since the optimal head group area is influenced by variables such as surface charges or solution conditions, the spontaneous curvature can be related to these variables. We find that Π_{ent}, Π_{rep} and Π_{corr} influence the spontaneous curvature simultaneously. Among them, Π_{corr} can be dominant for certain range of variables. It efficiently modifies and even changes the sign of the spontaneous curvature. As our microscopic model is different from previous models using PB equations [63–66], a comparison between the spontaneous curvature obtained in these two models will be discussed.

4.5.1 Effects of charge correlations

Fig. 4.1 shows C_0 as a function of charge fraction on the inner leaflet, α, and sodium concentration, [Na^+]. We choose the parameters $a_0^{out} = a_0 = 80\mathring{A}^2$, $D = 2l_s = 4\ nm$, and $v_0 = a_0 l_s = 1.6\ nm^3$. Since σ_0 is expressed in terms of charge fraction α: $\sigma_0 = \alpha/a_0^{in}$, the charge asymmetry of the bilayer, $\Delta\sigma = \sigma_0$, can be represented by α. In the presence of monovalent counterions only (Fig. 4.1 (a) and (c)), the value of C_0 changes non-monotonically and is negative for weakly charged surface at low salt concentrations. However, C_0 turns positive for larger α and larger [Na^+]. This can be attributed to the behavior of $\Delta\Pi$. For weakly charged surface at low salt concentration, the entropy of counterion release, $\Delta\Pi_{ent}$, dominates $\Delta\Pi$ and tends to expand the inner leaflet, leading to a negative C_0. As α or [Na^+] increases, correlations between surface charges and condensed counterions become important and tend to shrink the inner leaflet. Thus C_0 turns positive.

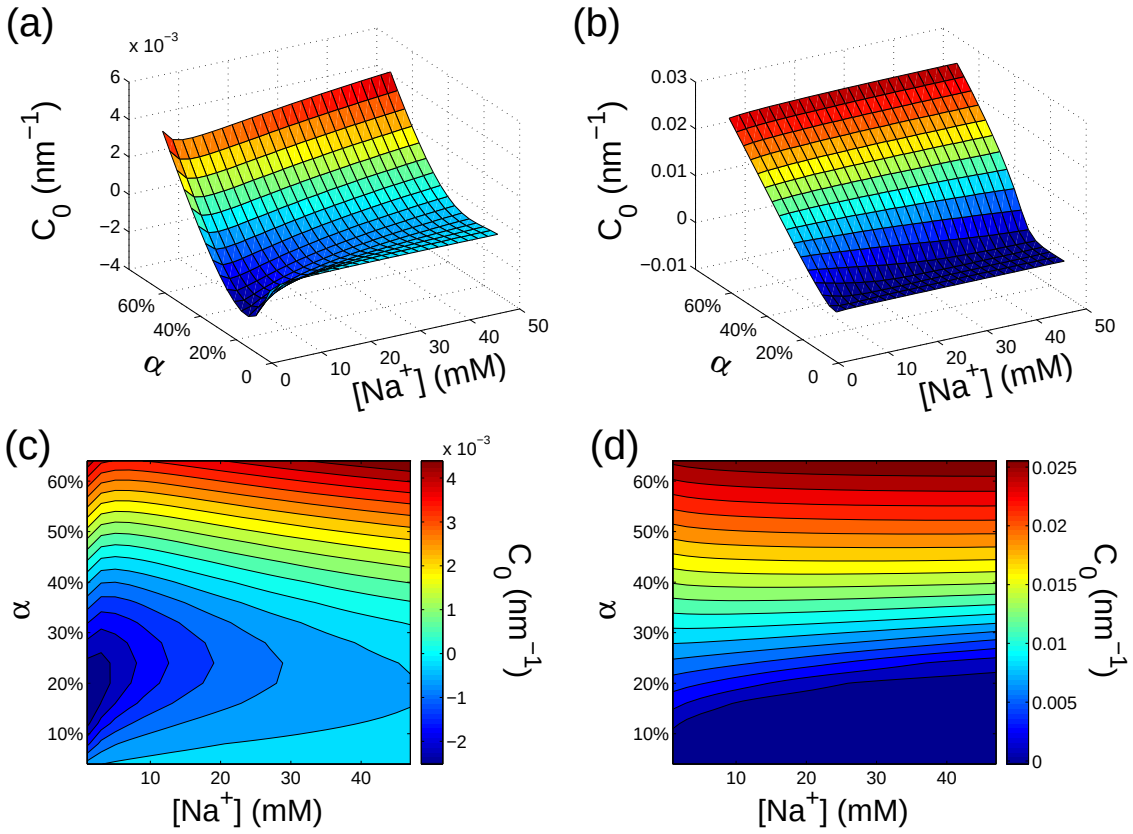

Figure 4.1: The spontaneous curvature C_0 of the asymmetrically charged bilayer as a function of sodium concentration in millimole, [Na^+], and surface charge fraction α. (a) Three-dimensional plot of C_0 in the absence of divalent counterions. (b) Three-dimensional plot of C_0 in the presence of 0.1 mM divalent counterions. (c) Contour plot of C_0 in the absence of divalent counterions. (d) Contour plot of C_0 in the presence of 0.1 mM divalent counterions. In (a) and (c), the spontaneous curvature C_0 is negative for smaller α and [Na^+] but turns positive for larger α and [Na^+]. In (b) and (d), C_0 remains positive for a wider range of α and [Na^+].

The effect of adding multivalent salts is also shown in Fig. 4.1 (b) and (d). In the presence of 0.1 mM divalent counterions such as Ca^{2+}, the spontaneous curvature remains positive for a wide range of parameters and is much larger in magnitude than the monovalent case. This is because the correlation contribution, which favors positive C_0, is greatly enhanced and dominates the entropic effect in the presence of divalent counterions unless α is too small. Thus we conclude that positive spontaneous curvature can be induced by charge correlations, an effect that becomes important for large α or high valency, and is more sensitive to counterion valency than to $[Na^+]$. As our C_0 arises from ΔA_0, the discussion about them is parallel.

4.5.2 Comparison to PB results at the mean-field level

We have developed a model to describe the spontaneous curvature of an asymmetrically charged bilayer. In that model, the spontaneous curvature is induced by the change in the optimal head group area due to interactions between charged head groups and counterions. Such interactions modify the spontaneous curvature in a bending-independent way in the sense that they do not depend on curvature state of the bilayer. On the other hand, the distance between two lipid head groups in a curved bilayer is shorter than in a planar one. Therefore, the interaction between two head groups may be influenced by curvature, leading to a contribution to the spontaneous curvature. Obviously, this contribution, which will be referred to as bending-induced spontaneous curvature, has not been captured in the our microscopic model. However, such contribution is calculated in the previous models for spherical or cylindrical symmetry, either within the Debye-Hückel (DH) approximation [6] or within the mean-field Possion-Boltzmann (PB) approximation [62, 63].

Which contribution to spontaneous curvature is dominant remains unknown so far. To answer this question, we compare C_0 obtained in our model to that in the PB approx-

imation at the mean-field level. We apply the two models to a cylindrical lipid bilayer in salty solution. This bilayer is the same as we considered in Section 4.4. In our microscopic model, the optimal head group area of the inner leaflet, $a_0^{in} = a_0^*$, can be modified by electrostatics. In the PB model,

$$a_0^{in} = a_0^{out} = a_0, \tag{4.35}$$

and thus

$$c_0^{in} = c_0^{out} = 0, \tag{4.36}$$

as bending does not change the optimal head group area. The curvature free energy per unit area of such a bilayer in the PB model is

$$G = g_m + g_{el}, \tag{4.37}$$

where g_m is the nonelectrostatic (mechanical) contributions to the curvature free energy and g_{el} is the electrostatic contribution.

The mechanical curvature free energy per unit area can be written as

$$g_m = \frac{k_m}{2R^2}, \tag{4.38}$$

where R is the radius of the mid-plane of the bilayer and k_m is the mechanical bending rigidity. Experimentally measured values of the mechanical bending rigidity k_m are summarized in [5]. Their values lie between 2 and 100 k_BT. The mechanical bending rigidity can also be related to the microscopic parameters in our model. If we choose $a_0^{in} = a_0^{out} = a_0$ and $H^m = 1/2R$ in Eq. 4.27 and compare it with Eq. 4.38, we find

$$k_m = \frac{k_s v_0^4}{2a_0^5}. \tag{4.39}$$

In the limit of $\kappa R \gg 1$ (κ^{-1} is the Debye length), the electrostatic part of the curvature free energy was derived analytically as an expansion in terms of $1/\kappa R$ in the mean-field

Poission-Boltzmann approach [62, 63]. For the bilayer in our case, the free energy per unit area on the mid-plane is

$$g_{el} = g_0 + \frac{g_1}{R} + \frac{g_2}{R^2}, \tag{4.40}$$

where

$$g_0 = k_B T \sigma_0 \left[2 \ln \left(\frac{s}{2} + \sqrt{1 + \frac{s^2}{4}} \right) - \frac{4}{s} \left(\sqrt{1 + \frac{s^2}{4}} - 1 \right) \right], \tag{4.41}$$

$$\begin{aligned} g_1 = & \frac{k_B T}{\pi l_B} \ln \left(\frac{1 + \sqrt{1 + \frac{s^2}{4}}}{2} \right) \\ & - k_B T \sigma_0 D \left[\ln \left(\frac{s}{2} + \sqrt{1 + \frac{s^2}{4}} \right) - \frac{2}{s} \left(\sqrt{1 + \frac{s^2}{4}} - 1 \right) \right], \end{aligned} \tag{4.42}$$

$$g_2 = \frac{k_B T \sigma_0}{\kappa^2} \left(\frac{1}{s} - \frac{8}{s^3} + \frac{8}{s^3 \sqrt{1 + \frac{s^2}{4}}} \right), \tag{4.43}$$

where

$$s = \frac{4 \pi l_B \sigma_0}{\kappa}. \tag{4.44}$$

The total free energy per unit area, G, is

$$G = g_0 + \frac{g_1}{R} + \frac{g_2 + \frac{k_m}{2}}{R^2} \tag{4.45}$$

The bending-induced spontaneous curvature is

$$C_0^{PB} = - \frac{g_1}{2 k_m + 4 g_2}. \tag{4.46}$$

The spontaneous curvature C_0 and C_0^{PB}, calculated in our microscopic model and in the PB model respectively, are shown in Fig. 4.2 as a function of $[Na^+]$ in the presence of monovalent counterions. Here we choose $\sigma_0 = 0.2$ nm^{-2}. The magnitude of σ_0 will change as the optimal head group area of the inner leaflet is modified by electrostatics. But as we have shown in the earlier chapter, the change in σ_0 can be ignored in the case of monovalent counterions. We choose $k_m = 20\ k_B T$ and $k_m = 50\ k_B T$. For $k_m = 20\ k_B T$,

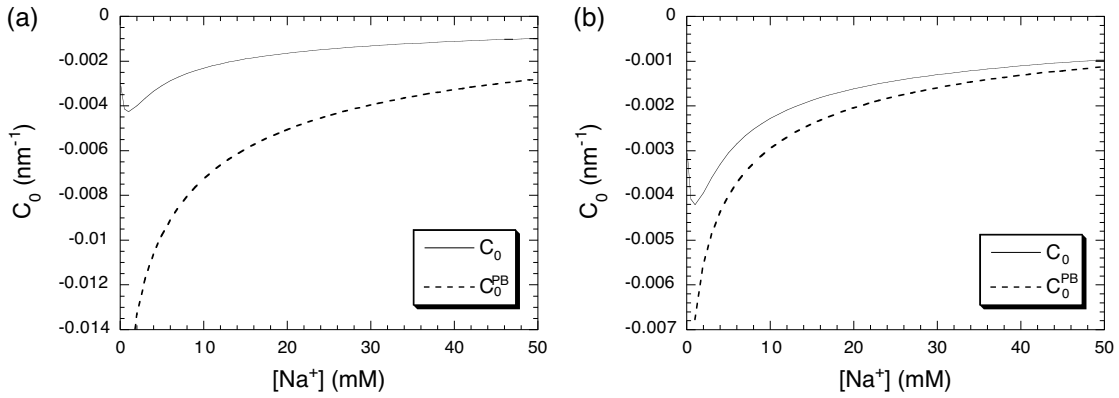

Figure 4.2: Comparison between our microscopic C_0 (solid line) and bending-induced C_0^{PB} (dashed line) as a function of sodium concentration in millimole, [Na^+], for different mechanical bending rigidity k_m, in the presence of monovalent counterions only. We choose $\sigma_0 = 0.2$ nm^{-2}. (a) For $k_m = 20\ k_BT$, C_0^{PB} is dominant over C_0. (b) For $k_m = 50\ k_BT$, C_0^{PB} and C_0 become comparable to each other.

C_0^{PB} is much larger than C_0. For $k_m = 50\ k_BT$, C_0^{PB} is reduced while C_0 is roughly independent of k_m. The two contributions become comparable. The difference between C_0 and C_0^{PB} can be attributed to the way k_m is treated in each model. In our model, electrostatics modifies C_0 as well as the mechanical properties of the bilayer, i.e., the optimal head group area, and influence k_m through this. In the PB model, however, the electrostatic contributions are independent of mechanical properties. In other words, k_m is not affected by electrostatics but can be arbitrarily assigned. The PB model leaves behind the question how k_m is determined by the microscopic properties. A better understanding of these two contributions shall benefit from clarification of this question.

Our above discussion of the two contributions has been limited to the mean-field level. Charge correlations, however, are expected to be important under certain conditions and may even change the sign of the spontaneous curvature. We cannot obtain a full picture of electrostatics of the spontaneous curvature unless charge correlations are considered.

Unfortunately, charge correlations in the bending-induced electrostatic contribution have not been fully explored, not even for spherical or cylindrical geometry. It is desirable to develop theories that capture both contributions simultaneously. Investigation along this line is warranted.

Chapter 5

Conclusions

In this thesis, we have theoretically studied the binding and bending of charged lipid bilayers. Lipid bilayers are typically charged in aqueous solution. They can electrostatically interact with each other, with ions and with other charged molecules.

To understand the effect of ionic sizes and the electrostatic attraction between like charged bilayers, we have developed a theoretical formalism in which ions are treated as charged hard spheres as in the restricted primitive model of a simple ionic fluid. We have used a two-dimensional Debye-Hückel approach to this system and found that attraction between two charged bilayers can be dramatically modified and enhanced by the nonzero ionic size in the case of physical interest ($h \gtrsim 5$Å). A plausible reason for this is that the in-plane charge distribution becomes more heterogeneous as the ionic size increases, resulting in a larger charge polarity and hence an enhanced attraction. Also the attraction gets stronger as the surface charge density σ_0 increases, implying that the ionic size influences the σ_0 dependence of the attraction. In other words, the effects of ionic sizes and the σ_0-dependence of the attraction are coupled to each other—the attraction is more sensitive to σ_0 for larger D.

Our results are consistent with the long-standing observation of enhanced attractions for high charge densities or large valency and also predicts more realistic results for the pressure that remains finite as $h \to 0$. The main advantage of our approach is that it allows us to systematically study the correlation attraction, without relying on additional approximations/assumptions besides linearization that might obscure the essential physics of correlation attractions.

We have also studied the electrostatics that regulates the preferred curvature of an asymmetrically charged bilayer: the relaxed area difference ΔA_0 and the spontaneous curvature C_0.

Based on the idea that the optimal areas of head groups are governed by opposing forces, we first have determined the optimal head group area a_0^* of an asymmetrically charged bilayer in salty solution by minimizing interfacial free energy at the lipid-water interface. In this way, we have mapped a_0^* onto experimentally measurable parameters such as the sodium concentration $[Na^+]$ and the charge fraction α.

By solving for a_0^*, we are able to analyse Δa_0^{in}, the change in the area of the inner leaflet, in a wider parameter range. We find the behavior of Δa_0^{in} can be attributed to the competition of three distinct contributions to $\Delta\Pi$: the entropy of counterion release from the bilayer, Π_{ent}, electrostatic repulsion Π_{rep}, and charge correlations Π_{corr}. Among them, Π_{ent} is dominant for small α at low $[Na^+]$ and is responsible for the positive value and the non-monotonic behavior of Δa_0^{in}. However, Π_{corr} counterbalances Π_{ent} in the presence of divalent counterions and efficiently shrink the inner leaflet, leading to negative Δa_0^{in} roughly independent of $[Na^+]$.

Inspired by a microscopic model for lipid monolayers, we have developed a formalism to relate the spontaneous curvature of a bilayer to a few microscopic parameters such as the optimal head group area, equilibrium chain length, and chain volume. Then we apply

this model to an asymmetrically charged bilayer and describe the spontaneous curvature C_0 in terms of salt concentrations and charge fractions, and thus are able to discuss electrostatics that governs the behavior of C_0.

As we did with ΔA_0, we have explained the behavior of C_0 in different solution conditions in terms of Π_{ent}, Π_{rep} and Π_{corr}. Our calculation indicates that asymmetry in surface charges or solution conditions can induce a nonzero spontaneous curvature, consistent with previous calculations at the mean-field level. In addition, our model has captured charge correlations that can have a significant effect on C_0 in the presence of multivalent counterions.

We have also compared our results with those in the PB approach at the mean field level. We find the difference between these two can be attributed to the way electrostatics influences the mechanical bending rigidity k_m: in our model, k_m can be modified by electrostatics through a_0^*; in the PB approach, k_m is independent of electrostatics, leaving behind the question how k_m is determined by the microscopic properties. Another unexplored problem is the contribution of charge correlations to the bending-induced spontaneous curvature. Our analysis cannot be realistic unless this problem is fully addressed. It is desirable that our C_0 could be combined with bending-induced C_0 and be applied to cell shape calculations.

Bibliography

[1] Gelbart et al., *Physics Today*, Sep. p38, 2000.

[2] V. A. Bloomfield, Biopolymers **31**, 1471 (1991); V. A. Bloomfield, Curr. Opin. Struct. Biol. **6**, 334 (1996).

[3] D. E. Leckband, C. A. Helm, and J. Israelachvili, Biochemistry **32**, 1127 (1993).

[4] D. Bratko, B. Jönsson, H. Wennerström, Chem. Phys. Lett. **128**, 449 (1986); R. Kjellander,T. Akesson, B.Jönsson, S. Marčelja, J. Chem. Phys. **97**, 1424 (1992).

[5] D. Boal, *Mechanics of the Cell* (Cambridge, 2002).

[6] M. Winterhalter and W. Helfrich, J. Phys. Chem. **92**, 6865 (1988).

[7] E. Ponder, *Hemolysis and Related Phenomena* (Grune & Stratton, New York, 1948).

[8] M. Bessis, *Living Blood Cells and Their Ultrastructure* (Springer, New York, 1973).

[9] T. L. Steck, in *Cell Shape: Determinants, Regulation, and Regulatory Role*, edited by W. Stein and F. Bronner (Academic, San Diego, 1989).

[10] J. Israelachvili, *Intermolecular and Surface Forces, 2nd Ed.* (Academic Press, 1992), Chap. 12.

[11] P. Wong, J. Theor. Biol. **196**, 343 (1999).

[12] G. S. Manning, J. Chem. Phys. **51**, 924 (1969).

[13] L. Miao, et al, Phys. Rev. E **49**, 5389 (1994).

[14] H. Dobereiner, et al., Phys. Rev. E **55**, 4458 (1997).

[15] H. Dobereiner, et al., Eur. Biophys. J. **28**, 174 (1999).

[16] J. X. Tang, S. Wong, P. Tran, and P. Janmey, Ber. Bunsen-Ges. Phys. Chem. **100**, 796 (1996).

[17] F. Oosawa, *Polyelectrolytes* (Marcel, Dekker, New York, 1971).

[18] B.-Y. Ha and A. J. Liu, in *Physical Chemistry of Polyelectrolytes*, edited by T. Radeva (Marcel Dekker, NY, 2001), p. 163.

[19] S. Marcelja, Biophys. J. **61**, 1117 (1992).

[20] P. Attard, R. Kjellander, D. J. Mitchell, and B. Jonsson, J. Chem. Phys. **89**, 1664 (1988).

[21] P. Attard, R. Kjellander, and D.J. Mitchell, Chem. Phys. Lett. **139**, 219 (1987); P. Attard, D. J. Mitchell, and B. W. Ninham, J. Chem. Phys. **88**, 4987 (1988).

[22] J. L. Barrat and J. F. Joanny, Adv. Chem. Phys. **94**, 1 (1996).

[23] P. A. Pincus and S. A. Safran, Europhys. Lett. **42**, 103 (1998).

[24] A. Sain and B.-Y. Ha, Physica A **320**, 67 (2003).

[25] D. B. Lukatsky and S. A. Safran, Europhys. Lett. **60**, 629 (2002).

[26] M. Kardar and R. Golestanian, Rev. Mod. Phys. **71**, 1233 (1999).

[27] I. Rousina and V. A. Bloomfield, J. Phys. Chem. **100**, 9977 (1996).

[28] B.-Y. Ha and A. J. Liu, Phys. Rev. Lett. **79**, 1289 (1997).

[29] B. I. Shklovskii, Phys. Rev. Lett. **82**, 3268 (1999).

[30] J. J. Arenzon, J. F. and Y. Levin, Eur. Phys. J. B **12**, 79 (1999).

[31] B.-Y. Ha, Phys. Rev. E **64**, 31507 (2001).

[32] A. W. C. Lau, P. Pincus, Dov Levine, and H. A. Fertig, Phys. Rev. E **63**, 51604 (2001).

[33] A. Moreira and R. R. Netz, Phys. Rev. Lett. **87**, 78301 (2001).

[34] A. Moreira and R. R. Netz, Eur. Phys. J. E **8**, 33 (2002).

[35] N. Gronbech-Jensen, R. J. Mashl, R. F. Bruinsma, and W. M. Gelbart, Phys. Rev. Lett. **78**, 2477 (1996).

[36] Guldbrand et al., J. Chem. Phys. **80**, 2221 (1984).

[37] E. S. Velazquez and L. Blum, Physica A **244**, 453 (1997).

[38] D. A. Mcquarrie, *Statistical Mechanics* (Harper & Row, New York, 1971), Chap. 15.

[39] In a low-salt limit, this can be easily satisfied.

[40] L. D. Landau and E. M. Lifshitz, *Statistical Physics, 3rd Ed. Part 1* (Pergamon Press, 1980), Chap. VII.

[41] R. N. Bracewell, *The Fourier Transform and Its Applications*, 3rd ed. (McGraw Hill, Boston, 2000), p. 338, Table 13.2.

[42] R. Kjellander and S. Marcelja, J. Phys. Chem. **90**, 1230 (1986).

[43] P. Canham, J. Theor. Biol. **26**, 61 (1970).

[44] W. Helfrich, Z. Naturforsch. **C28**, 693 (1973).

[45] H. J. Deuling and W. Helfrich, J. Phys. (Paris) **37**, 1335 (1976).

[46] B. Deuticke, Biochim. Biophys. Acta. **163**, 494 (1968); N. Mohandas and C. Feo, Blood Cells. **1**, 375 (1975); J. Smith, et al., Am. J. Vet. Res. **43**, 1041 (1982).

[47] A. Herrmann, P. Müller and R. Glaser, Biosci. Rep. **5**, 417 (1985).

[48] T. Tanaka, et al., Biochem. Biophys. Acta **1564**, 173 (2002).

[49] Y. Lange and J. Slayton, J. Lipid Res. **23**, 1121 (1982).

[50] M. Rasia and A. Bollini, Biochem. Biophys. Acta **1372** 198 (1998).

[51] S. Svetina, et al., Stud. Biophys. **110**, 177 (1985).

[52] J. Gimsa, Biophys. J. **75**, 568 (1998).

[53] M. Sheetz and S. Singer, Proc. Natl. Acad. Sci. USA **71**, 4457 (1974).

[54] P. Zarda, et al., J. Biomech. **10**, 211 (1977).

[55] C. Tanford, *The Hydrophobic Effect* (Wiley, New York, 1980).

[56] V. A. Parsegian, Trans. Faraday Soc. **62**, 848 (1966); R. E. Weast, *Handbook of Chemistry and Physics*, 50th ed. (CRC Press, Boca Raton, 1970).

[57] B.-Y. Ha, Phys. Rev. E **67**, 030901 (2003).

[58] S. Alexander, et al., J. Chem. Phys. **80**, 11 (1984).

[59] S. A. Safran, *Sratistical Thermodynamics of Surfaces, Interfaces, and Membranes* (Addison-Wesley, Reading, 1994).

[60] L. Miao, et al., Phys. Rev. A **43**, 6843 (1991).

[61] U. Seifert, et al., Phys. Rev. A **44**, 1182 (1991).

[62] H. N. W. Lekkerkerker, Physica A **159**, 319 (1989).

[63] D. J. Mitchell and B. W. Ninham, Langmuir **5**, 1121 (1989).

[64] M. Winterhalter and W. Helfrich, J. Phys. Chem. **96**, 327 (1992).

[65] A. Fogden, D. J. Mitchell and B. W. Ninham, Langmuir **6**, 159 (1990).

[66] T. Chou, et al., Biophys. J. **72**, 2042 (1998).